LASER INTERFEROMETER GRAVITATIONAL WAVE OBSERVATORY
– LIGO –
CALIFORNIA INSTITUTE OF TECHNOLOGY
MASSACHUSETTS INSTITUTE OF TECHNOLOGY

DOCUMENT TYPE LIGO-T000097-00-R 9/1/00

Understanding the LIGO Optics Suspension Controller Electronics Design

Ivica Stevanovic, Alan Weinstein

Distribution of this draft:

This is an internal working note
Of the LIGO Project
WWW: http://www.ligo.caltech.edu

California Institute of Technology
LIGO Project – MS 51-33
Pasadena, CA 91125
Phone (626)395-2129
Fax (626)304-9834
E-mail: info@ligo.caltech.edu

Massachusetts Institute of Technology
LIGO Project – MS 20B-145
Cambridge, MA 01239
Phone (617)253-4824
Fax (617)253-7014
E-mail: info@ligo.mit.edu

UNDERSTANDING THE LIGO OPTICS SUSPENSION CONTROLLER ELECTRONICS DESIGN

Student: Ivica Stevanovic, School of Electrical Engineering, University of Belgrade

Mentor: Prof. Dr. Alan J. Weinstein

ABSTRACT

The test masses in interferometer are subject to lots of noise: seismic noise (from the environment), thermal noise, shot noise due to quantum-mechanical nature of light. In order to approximate the condition of test masses falling freely and to isolate them from the noisy laboratory environment, a pendulum suspension is used. A pendulum suspension is a vibration isolator, which acts as a low pass filter for motion. By itself, that isn't good enough, so optics suspension controllers are used to sense and control the position of test masses. The position, pitch, yaw and side degrees of freedom of suspension system are sensed via LEDs and photo diodes, and then, through the electronics circuitry in negative feedback, they are corrected. The position degree of freedom must be controlled in order to maintain cavity resonance, and pitch, yaw, input beam position and direction must be controlled in order to maintain only the TEM_{00} mode of the laser beam. This project mostly consists of Matlab and Simulink time and frequency domain modeling of optic suspension electronics design that will be used in the upgraded LIGO prototype 40-meter interferometer concerning noise requirements and stability of the control system.

1. INTRODUCTION

In the first section of this report the equations of motion for position, pitch and yaw degrees of freedom of a suspended mirror are derived. The Simulink model of a pendulum is introduced and the main features of it are shown.
In the second section the LIGO 40m optics suspension controller electronics design is explained.
In the third section the Simulink model of a pendulum with negative feedback servo is introduced and all good features of this model are shown on Bode plots and time domain diagrams.
In the forth section are shown the Bode plots of Digital LOS and SOS controller electronics design which is prepared (J. Heefner, R. Bork) to replace the existing analog one.
In the fifth section the issue of the electrostatic force acting on suspended test mass is addressed.

1.1 THE EQUATIONS OF MOTION FOR POSITION AND PITCH DEGREES OF FREEDOM OF A SUSPENDED MIRROR

Let us think about the pendulum system shaken horizontally as shown in Fig. 1. The mass M is suspended by the wire of the length d at the release point above the center of mass by distance d_p. Let x, θ and θ' denote the horizontal displacement of the center of the mass, the pitch angle of the mass and the pitch angle of the wire, respectively.

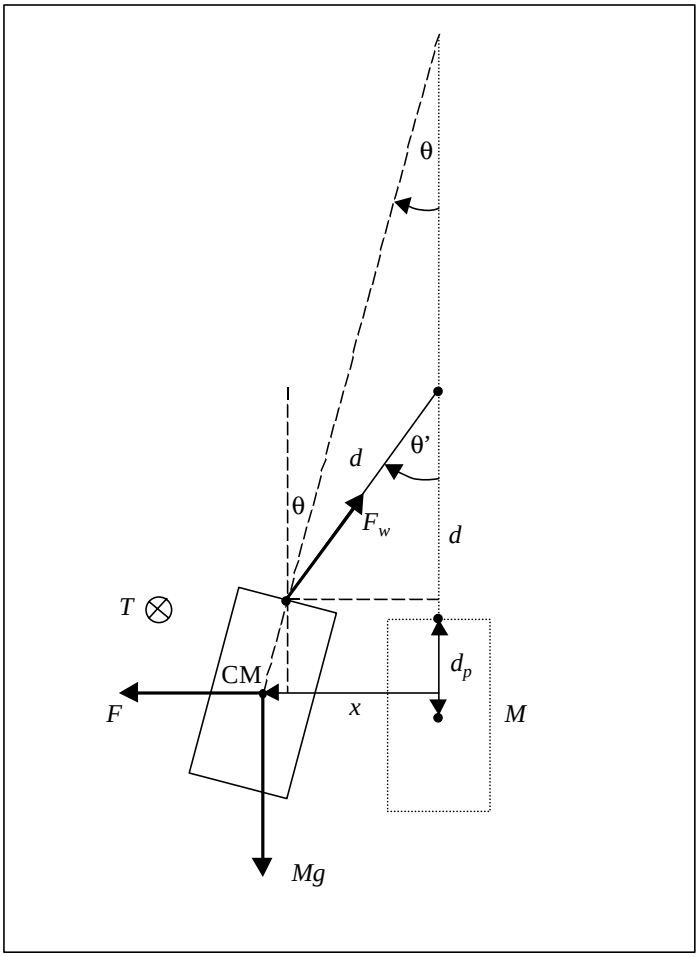

Figure 1.1 Response of the pendulum system to the horizontal motion of the suspension point

For very small displacement x from Fig. 1.1 we obtain the following

$$F_w \approx Mg\,, \tag{1-1}$$

$$x = d \cdot \theta' + d_p \cdot \theta\,, \tag{1-2}$$

$$\theta' = \frac{x - d_p \cdot \theta}{d_p}\,, \tag{1-2a}$$

where F_w is a wire tension force, and g is gravitational constant.

In horizontal direction the forces that act on a suspended mass are the external horizontal force F (it is inertial force due to horizontal motion of suspension point) and horizontal component of wire tension force. For equation of motion in horizontal direction we obtain

$$M\frac{d^2x}{dt^2} = F - F_w \sin\theta' \approx F - Mg\theta' = F - Mg\frac{x - d_p\cdot\theta}{d}, \tag{1-3}$$

$$M\frac{d^2x}{dt^2} = F - \frac{Mg}{d}x + \frac{Mgd_p}{d}\theta. \tag{1-3a}$$

Equation of motion for the torque T with respect to the center of mass of suspended mirror is as follows

$$I\frac{d^2\theta}{dt^2} = T + F_w \sin(\theta' - \theta)\cdot d_p \approx T + Mgd_p(\theta' - \theta) = T + Mgd\left(\frac{x - d_p\cdot\theta}{d} - \theta\right), \tag{1-4}$$

$$I\frac{d^2\theta}{dt^2} = T + \frac{Mgd_p}{d}x - \frac{Mgd_p(d_p + d)}{d}\theta, \tag{1-4a}$$

where I is moment of inertia for suspended test mass and T is external torque acting on the test mass and causing it to rotate in pitch degree of freedom.
From equations (1-3a) and (1-4a) it could be easily seen that if the test mass is displaced from equilibrium position by small horizontal displacement x and angular displacement in pitch degree of freedom θ, there will be restoring force and restoring torque acting on a test mass with force constant k_F and torque constant k_T which are given by

$$k_F = \frac{Mg}{d}, \tag{1-5a}$$

$$k_T = \frac{Mgd_p(d_p + d)}{d}. \tag{1-5b}$$

Therefore, the position and pitch resonance frequency of a suspended test mass are given by

$$f_x = \frac{1}{2\pi}\sqrt{\frac{k_F}{M}} = \frac{1}{2\pi}\sqrt{\frac{g}{d}}, \tag{1-6a}$$

$$f_\theta = \frac{1}{2\pi}\sqrt{\frac{k_T}{I}} = \frac{1}{2\pi}\sqrt{\frac{Mgd_p(d_p + d)}{I\cdot d}}, \tag{1-6b}$$

where moment of inertia of suspended test mass of diameter D and length L is given by

$$I = M\left(\frac{D^2}{16} + \frac{L^2}{12}\right). \tag{1-6c}$$

1.2 THE EQUATION OF MOTION FOR YAW DEGREE OF FREEDOM OF A SUSPENDED MIRROR

The yaw motion of the suspension point naturally causes the yaw motion of the mass (Fig 1.2).

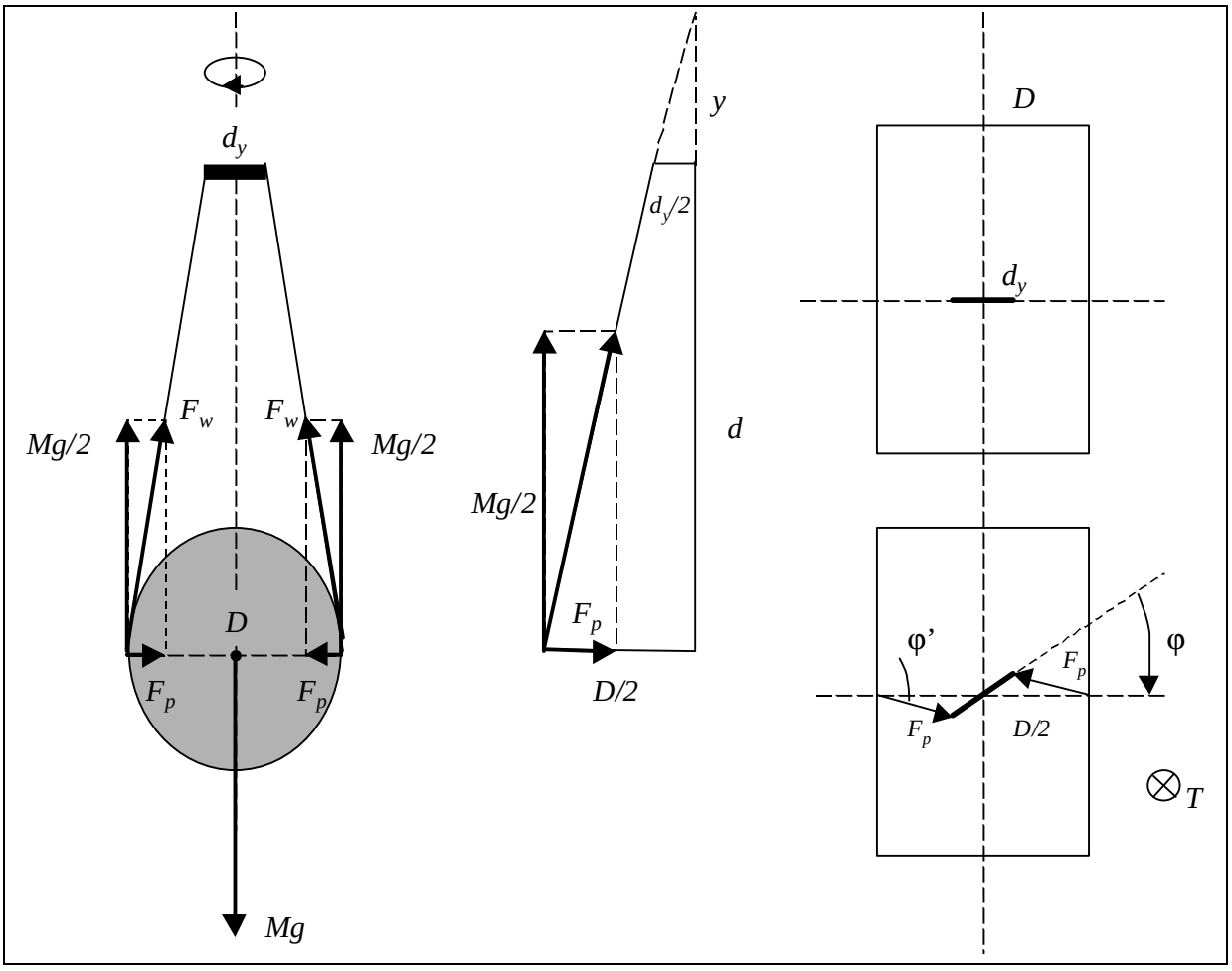

Figure 1.2 The yaw motion of the suspended test mass

For very small angle displacement in yaw degree of freedom φ, according to the sine theorem from Fig. 1.2 we obtain

$$\frac{D/2}{\sin(\pi-(\varphi+\varphi'))}=\frac{d_y/2}{\sin\varphi'}, \tag{1-7}$$

$$\frac{D}{\varphi+\varphi'}=\frac{d_y}{\varphi'}, \tag{1-7a}$$

$$\varphi'=\varphi\frac{d_y}{D-d_y}, \tag{1-7c}$$

where D is the diameter of suspended mirror and d_y is the distance between two suspension points of a single loop wire.

For horizontal component of a wire tension force, from Fig. 1.2 we obtain

$$F_p = \frac{Mg}{2}\tan\angle(\overrightarrow{F_w}, \vec{g}) = \frac{1}{4}Mg\frac{D}{d+y}, \tag{1-8a}$$

where $d + y$ is given by

$$d + y = \frac{d}{1-\frac{d_y}{D}} \tag{1-8b}$$

and hence

$$F_p = \frac{1}{4}MgD\cdot\frac{1-\frac{d_y}{D}}{d} = \frac{1}{4}Mg\frac{D-d_y}{d}. \tag{1-8c}$$

Equation of motion for the external torque T in yaw degree of freedom is as follows

$$I\frac{d^2\varphi}{dt^2} = T - F_p\sin\varphi'\cdot D \approx T - F_p D\cdot\varphi' = T - \frac{1}{4}MgD\frac{d_y}{d}\cdot\varphi. \tag{1-9}$$

Restoring torque acts on a suspended test mass, when it is displaced by a small yaw angle, with torque constant given by

$$k_T = \frac{MgD}{4}\frac{d_y}{d} \tag{1-10}$$

and therefore, the yaw resonance frequency is given by

$$f_\varphi = \frac{1}{2\pi}\sqrt{\frac{k_T}{I}} = \frac{1}{2\pi}\sqrt{\frac{MgD}{4I}\cdot\frac{d_y}{d}}. \tag{1-11}$$

The yaw motion of suspended test mass is not perfectly harmonic, since there are frictional forces that act on it. Therefore we have damped harmonic motion with damping torque proportional to angular velocity

$$T_d = -\gamma\frac{d\varphi}{dt} \tag{1-12a}$$

and the equation of motion is

$$I\frac{d^2\varphi}{dt^2} = T - k_T\cdot\varphi - \gamma\frac{d\varphi}{dt}. \tag{1-12b}$$

By taking the Laplace transform of both sides of this equation we obtain transfer function (torque to yaw angle)

$$\frac{\Phi(s)}{T(s)} = \frac{1/I}{s^2 + \frac{\gamma}{I}s + \frac{k_T}{I}}. \tag{1-12c}$$

The more general form of this transfer function is given by

$$\frac{\Phi(s)}{T(s)} = \frac{K}{s^2 + \frac{\omega_n}{Q} s + \omega_n{}^2}, \tag{1-12d}$$

where Q is the quality factor of the damped harmonic motion and shows how lossy oscillator is (the higher Q factor is, the less are the losses), and ω_n is natural resonance frequency that we would have if there weren't the damping torque acting on a test mass. It is obvious that

$$\omega_n = 2\pi f_\varphi \tag{1-12e}$$

and

$$Q = \frac{I\omega_n}{\gamma}. \tag{1-12f}$$

The resonance frequency of the damped harmonic motion is given by

$$f_\varphi' = \frac{1}{2\pi}\sqrt{\omega_n^2 - \left(\frac{\gamma}{2I}\right)^2} \approx f_\varphi \tag{1-12g}$$

for very high Q factor.

1.3 THE 40M TEST MASS AND SUSPENSION CONFIGURATION

The 40m test mass suspension is designed to accommodate a test mass with the following specifications:

- Size D = 101.6 mm = 4" in diameter and L = 88.9 mm = 3.5" in length
- Weight M = 1.6 kg
- Moment of inertia $I = 2.1\times10^{-3}$ kg m^2

The definitions of the parameters of the suspension configuration are shown in Fig. 1.3. The parameters of the suspension configuration, the pendulum, pitch and yaw resonance frequencies, calculated according to formulae derived in sections 1.1 and 1.2, are shown in Table 1.1. A single loop steel music wire is used to suspend the test mass. Its parameters are: density $\rho = 7.8\,\mathrm{g/cm^3}$, Young's modulus $Y = 2.1\times10^{11}$ N/m^2 and diameter $D_w = 91\,\mu\mathrm{m}$.

Parameters	*Designed Values*
d [mm]	350
d_p [mm]	1.3
d_y [mm]	26
Pendulum Resonance Frequency f_x [Hz]	0.84
Pitch Resonance Frequency f_θ [Hz]	0.5
Yaw Resonance Frequency f_φ [Hz]	0.6

Table 1.1 Parameters of suspension configuration

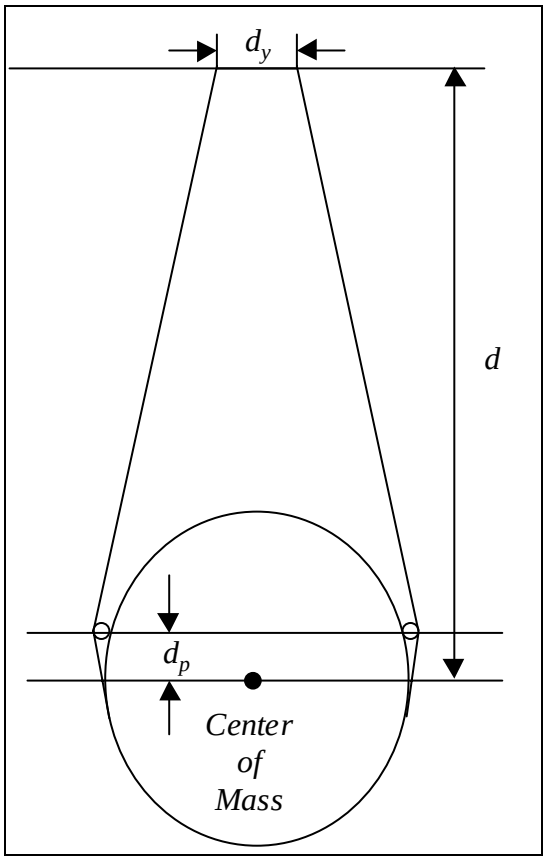

Figure 1.3 Definitions of parameters for the suspension configuration

1.4 SIMULINK MODEL OF A PENDULUM

We will first begin with Simulink model of a pendulum for yaw degree of freedom. We will rewrite the transfer function, derived before, in terms of zeros and poles, since that is the way the transfer functions are presented in Simulink. For the transfer function given by (1-12c) we obtain

$$\frac{\Phi(s)}{T(s)} = \frac{1/I}{(s+\alpha-j\omega_n)(s+\alpha+j\omega_n)}, \tag{1-13}$$

where α is given by

$$\alpha = \frac{\gamma}{2I} = \frac{\omega_n}{2Q} \tag{1-13a}$$

and the transfer function has two poles

$$p_{1/2} = -\alpha \pm j\omega_n . \tag{1-13c}$$

The Block diagram of a pendulum model for yaw degree of freedom is shown in Fig. 1.4.

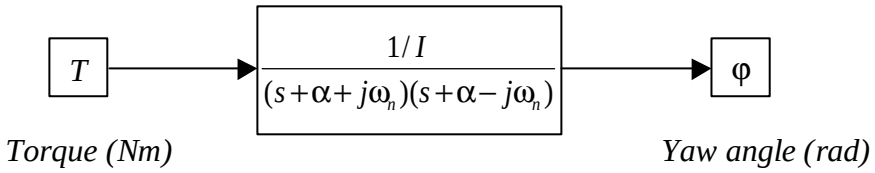

Figure 1.4 Block diagram of a pendulum for yaw degree of freedom

Taking into account parameters of the 40m test mass and suspension, the transfer function from torque to yaw is given by

$$\frac{\Phi(s)}{T(s)} = \frac{476.2}{(s+0.001+j2\pi 0.6)(s+0.001-j2\pi 0.6)}. \tag{1-14}$$

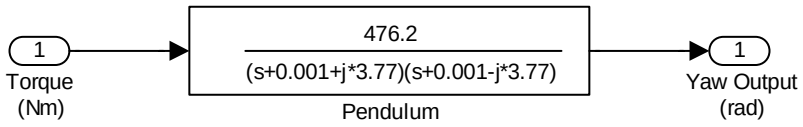

Figure 1.5 Simulink model of a 40m optical suspension for yaw degree of freedom

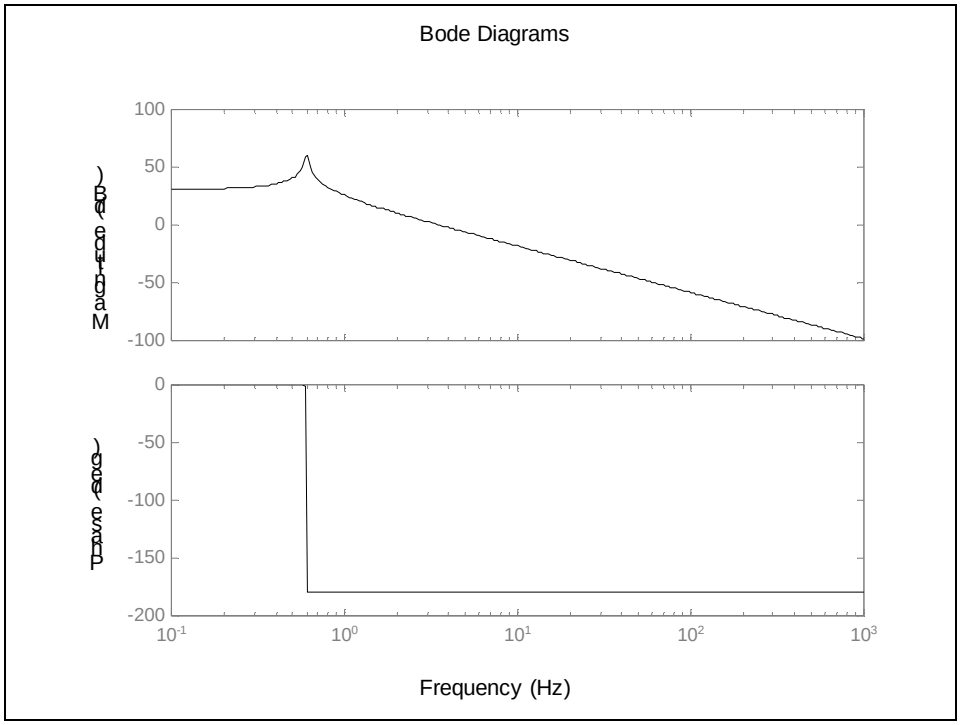

Figure 1.6 Bode diagrams of the transfer function of the 40 m pendulum for yaw degree of freedom

From Fig. 1.6 it can be easily seen that pendulum acts as a low pass filter for motion in yaw degree of freedom (and for position and pitch degrees of freedom also, which will be shown later). From this transfer function, however, we can not see what is the attenuation at low frequencies (below the yaw resonance frequency). It would be much better if we looked at yaw motion of suspension point to yaw motion of pendulum transfer function. Let φ_e denotes the yaw angle of the suspension point, and let φ, like before, denotes the yaw angle of the suspended mass. The external torque will be taken into account through the yaw motion of suspension point (it will be inertial torque acting on the test mass). Now (1-12b) can be written in as follows

$$I\frac{d^2\varphi}{dt^2} = -k_T(\varphi - \varphi_e) - \gamma\frac{d\varphi}{dt} \tag{1-15}$$

By taking Laplace transform of this equation, we obtain the transfer function from the yaw angle of the suspension point to the yaw angle of the mass

$$\frac{\Phi(s)}{\Phi_e(s)} = \frac{\frac{k_T}{I}}{s^2 + \frac{\gamma}{I}s + \frac{k_T}{I}} = \frac{\omega_n^2}{s^2 + \frac{\omega_n}{Q}s + \omega_n^2} \tag{1-15b}$$

Bode diagrams of this transfer function, obtained from Simulink model, are shown in Fig. 1.7.

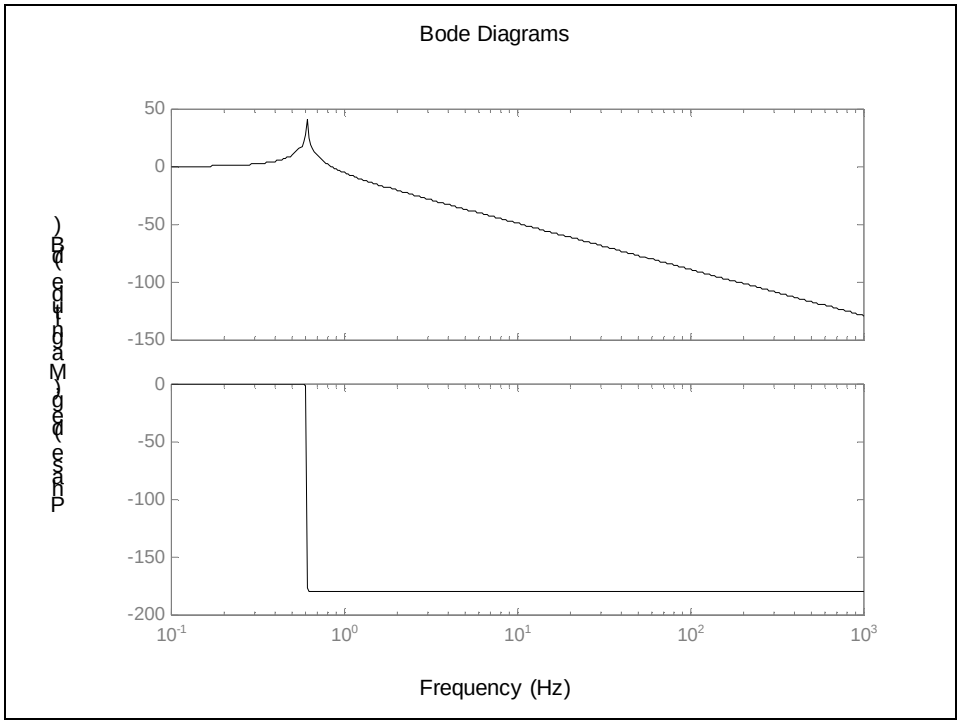

Figure 1.7 Bode diagrams of the modified transfer function for yaw degree of freedom

From this figure it can be easily seen that at lower frequencies (less than yaw resonant frequency which is 0.6 Hz) the yaw motion of test mass is without attenuation. For frequencies that are greater than yaw resonance frequency we have attenuation which increases for 40 dB over each decade. But at frequencies around the resonance frequency the yaw motion of test mass is amplified up to 30 dB relative to the yaw motion of suspension point. This is why velocity damping control is used, to introduce additional damping which will make the transfer function not to have bump around the resonance frequency.

We turn now to the position and pitch degrees of freedom. By taking the Laplace transform of (1-3a) and (1-4a) we obtain

$$Ms^2 X(s) = F(s) - \frac{Mg}{d} X(s) + \frac{Mgd_p}{d} \Theta(s) \tag{1-16a}$$

$$Is^2 \Theta(s) = T(s) + \frac{Mgd_p}{d} X(s) - \frac{Mgd_p(d_p + d)}{d} \Theta(s) \tag{1-16b}$$

Block diagram of the pendulum model for horizontal displacement and pitch degrees of freedom, according to (1-16(a)(b)) is shown in Fig. 1.8. From this diagram it can be easily seen that horizontal displacement and pitch angle of the pendulum are coupled. Bode diagrams of transfer functions from horizontal force to horizontal displacement and from torque to pitch angle are shown in Figures 1.10 and 1.11. Coupling in position and pitch degrees of freedom can be seen from these diagrams (we have a peak in position transfer function at pitch resonance frequency and vice versa).

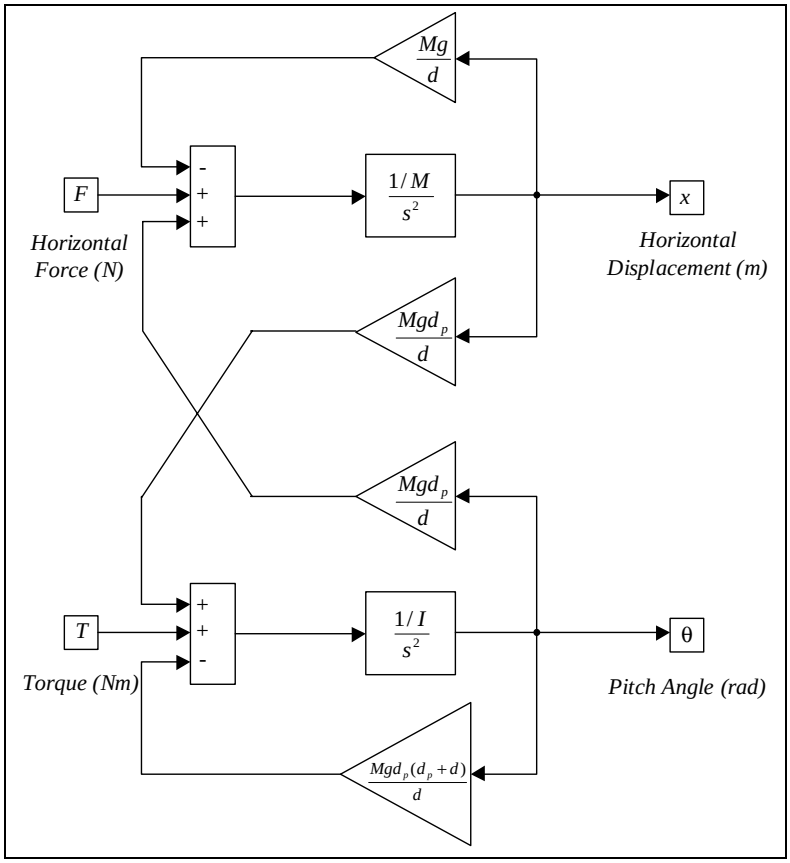

Figure 1.8 Block diagram of the pendulum for position and pitch degrees of freedom

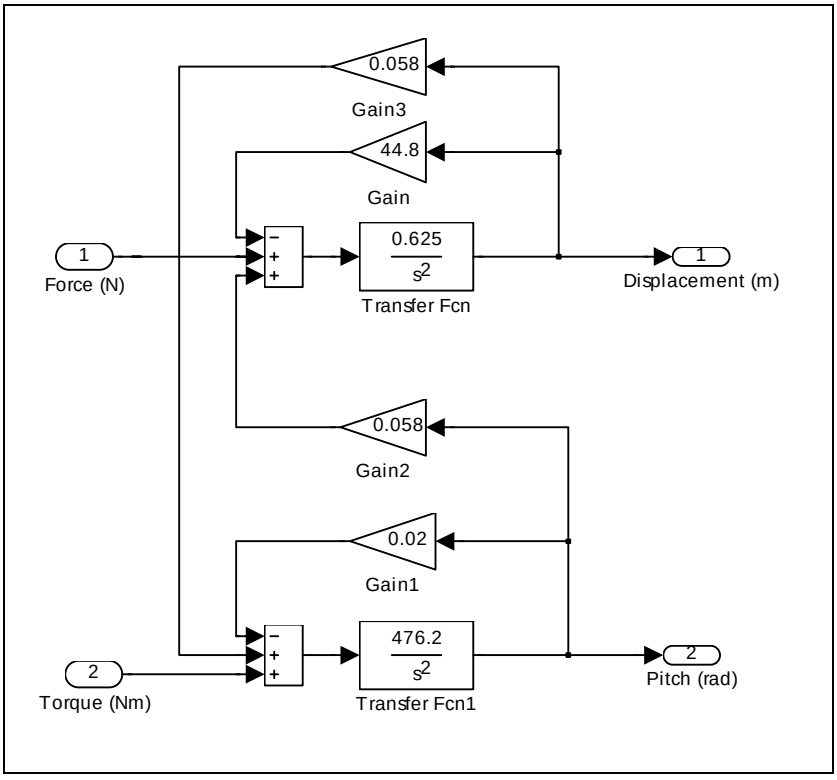

Figure 1.9 Simulink model of the 40 m optical suspension for position and pitch degrees of freedom

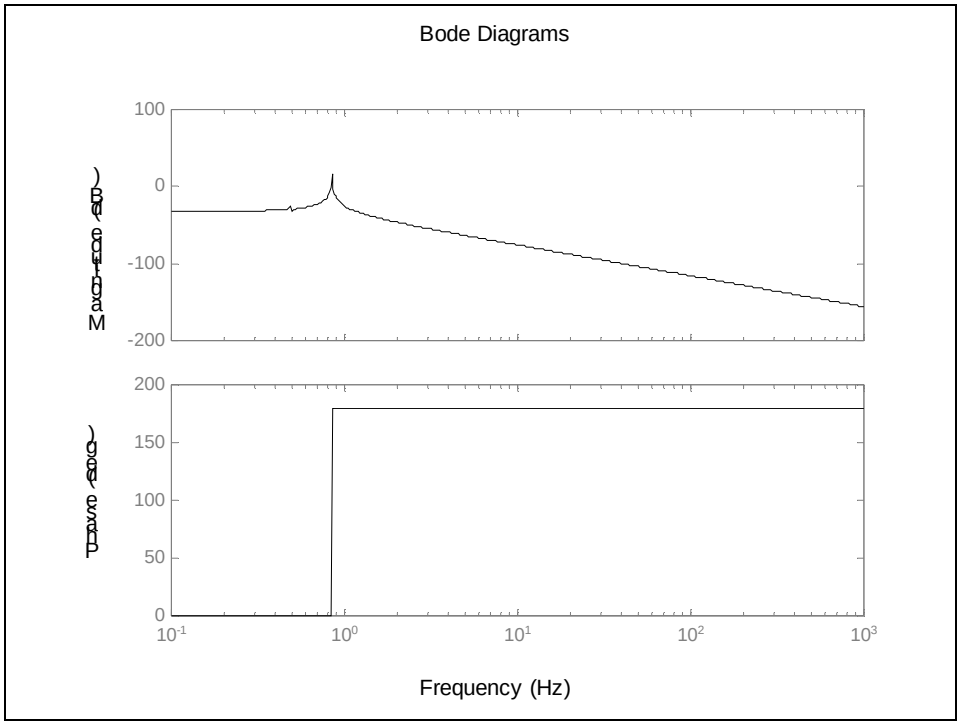

Figure 1.10 Bode diagrams of the transfer function of the 40 m pendulum from horizontal force to horizontal displacement

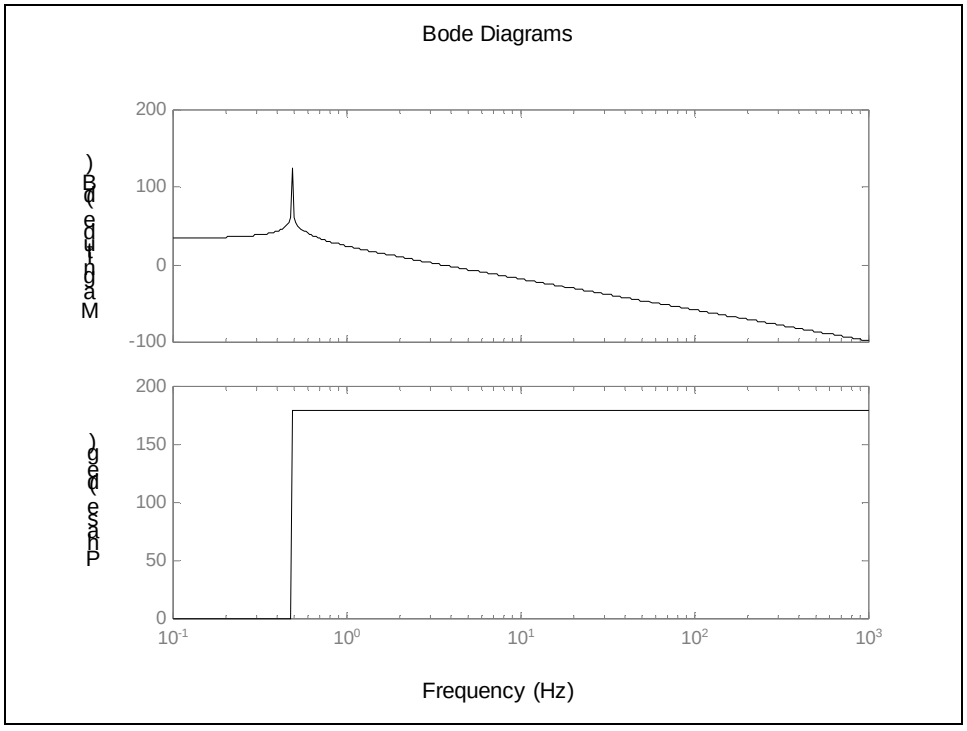

Figure 1.11 Bode diagrams of the transfer function of the 40 m pendulum from torque to pitch angle

In order to derive the transfer function from horizontal displacement of the suspension point, x_e, to the horizontal displacement of the test mass, x, and to the pitch angle of the test mass, θ, we'll look at Fig. 1.12.

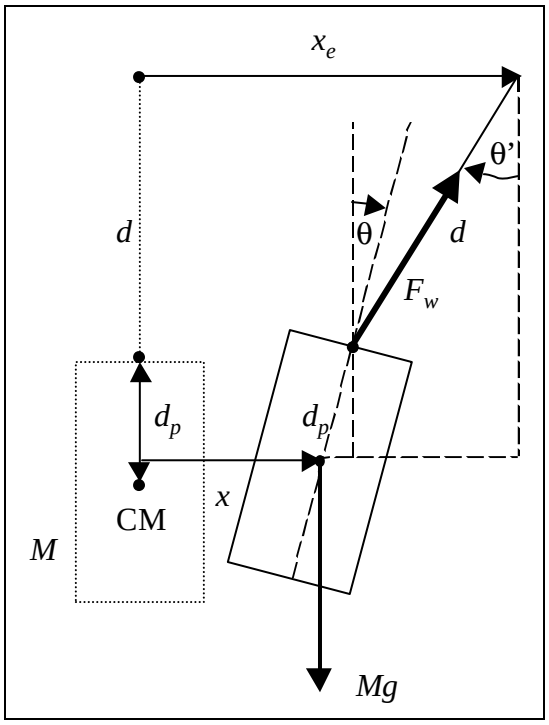

Figure 1.12 Response of the pendulum system to the horizontal motion of the suspension point

We obtain the following eqations

$$\theta' = \frac{x_e - x - d_p\theta}{d}, \tag{1-17a}$$

$$M\frac{d^2x}{dt^2} = F_w \sin\theta' \approx Mg\theta' = \frac{Mg}{d}(x_e - x - d_p\theta), \tag{1-17b}$$

$$I\frac{d^2\theta}{dt^2} = F_w d_p \sin(\theta' - \theta) \approx \frac{Mgd_p}{d}(x_e - x - d_p\theta - d\cdot\theta). \tag{1-17c}$$

In Laplace domain we obtain

$$s^2X(s) = \frac{g}{d}\left[X_e(s) - X(s) - d_p\Theta(s)\right], \tag{1-18a}$$

$$Is^2\Theta(s) = \frac{Mgd_p}{d}\left[X_e(s) - X(s) - d_p\Theta(s) - d\,\Theta(s)\right]. \tag{1-18b}$$

Block diagram, which reflects these two equations, is shown in Fig. 1.12.

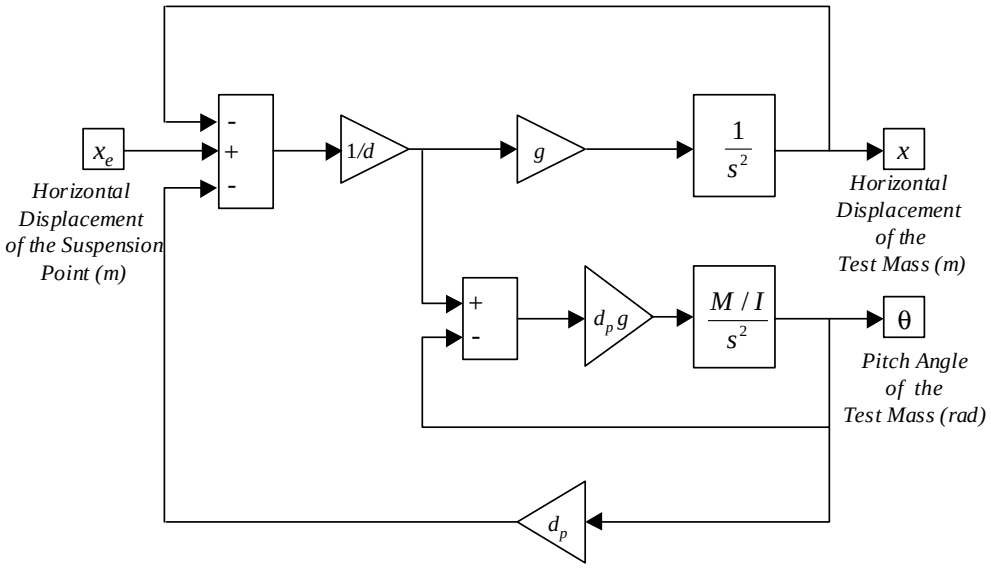

Figure 1.13 Block diagram reflecting the horizontal and pitch motion of the pendulum system with horizontal motion of the suspension point

The Bode diagrams show that there is no attenuation at DC, and that attenuation at higher frequecies is -40 dB/dec. Around the pendulum resonance frequency there is the amplification of motion which goes to 32 dB.

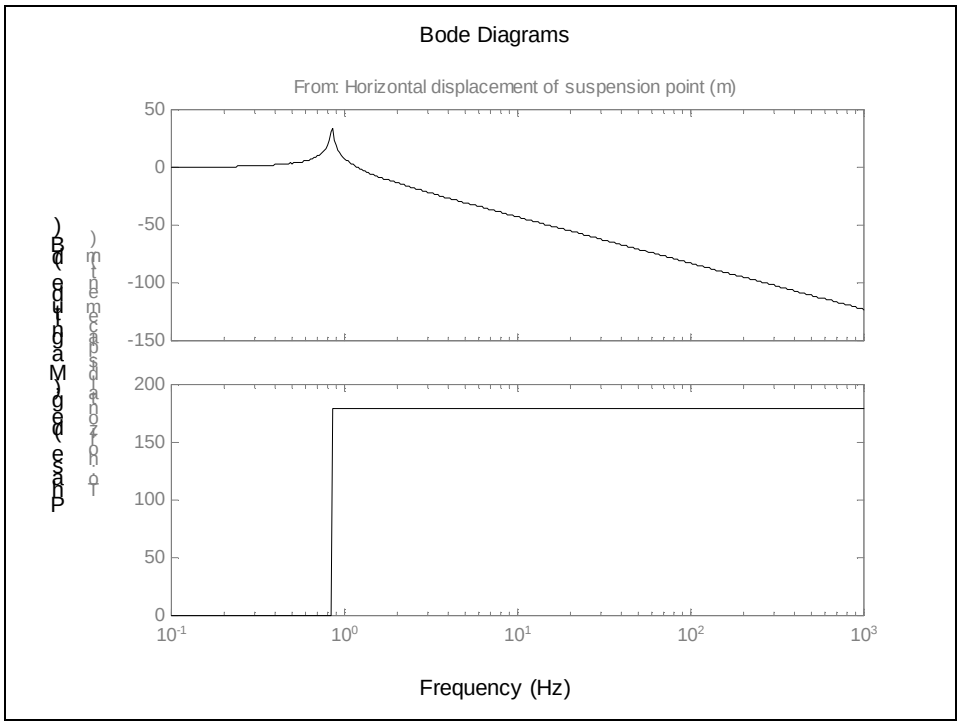

Figure 1.14 Bode diagrams of the transfer function of the 40 m pendulum from horizontal displacement of suspension point to horizontal displacement of the test mass

Obviously, the good feature of the pendulum is that the ground motion and all other disturbances are attenuated at frequencies greater than resonance frequency of the pendulum. Let the ground motion, i. e. the suspension point displacement be given by

$$x_e = A_1 \sin(2\pi f_1 t) + A_2 \sin(2\pi f_2 t), \tag{1-19}$$

where $A_1 = 1\,\mu\text{m}$, $A_2 = 0.1\,\mu\text{m}$, $f_1 = 0.1\,\text{Hz}$ and $f_2 = 10\,\text{Hz}$.
In Fig 1.15 the suspension point displacement versus time and the test mass displacement versus time (pendulum response) are shown. From these figures it can be seen that the ground motion component at 10 Hz is filtered out and that component at frequency 0.1 Hz remains. Since the pendulum resonates at resonance frequency of 0.84 Hz, we have a component induced at that frequency. In order to minimize the amplification of ground motion near the frequency of the pendulum resonance, velocity damping is used.

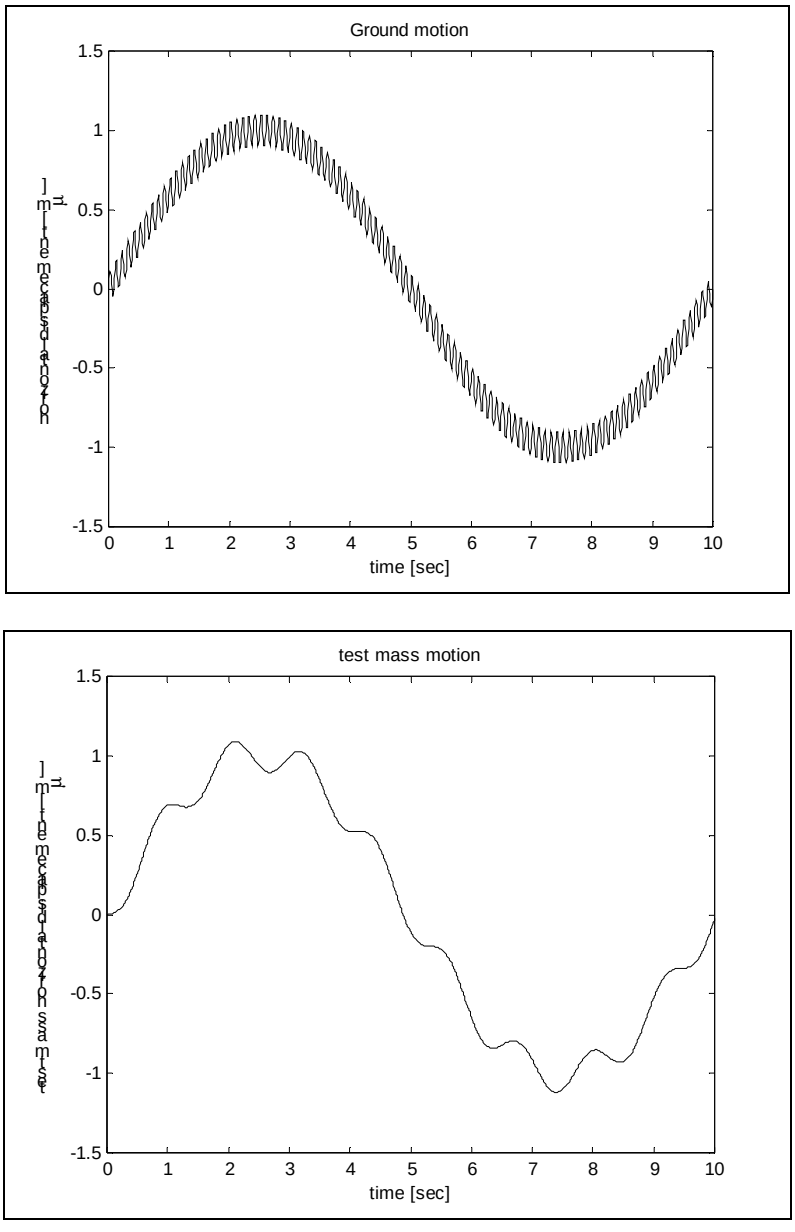

Figure 1.15 An example of pendulum response to ground motion

2. CONTROL SYSTEM DESIGN

A mass suspended as a pendulum from a tower is free in an inertial space at frequencies much larger than pendulum resonance frequency. Its displacement d at frequency f can be approximated by

$$d = d_t \left(\frac{f_0}{f} \right)^2 \tag{2-1}$$

where d_t is the displacement of the tower, i. e. the suspension point and f_0 is the pendulum resonance frequency. This is the idea behind suspending a mirror to isolate it from ambient vibration. The pendulum resonance frequency is around 1 Hz, thus there is vibration isolation of about 10^{-4} starting at 100 Hz, which is in our bandwidth of interest.

On the other hand, because the gravitational restoring force is lossless, the Q of the pendulum is high (~10^6), hence the mirror needs damping at its low frequency resonances to hold it steady for interferometry. OSEMs (Optical Sensor Electronic Motor) are used for this purpose. The purpose of these devices to sense and control suspended test mass motion at low frequencies, and not to involve additional disturbances at higher frequencies where performance of the pendulum is good enough. So, there are three major requirements that should be met in designing of the suspended test mass servo system:

1. The servo has to sense and control low frequency motion of the pendulum and to adequately suppress this motion. It is assumed that the sensor noise is much lower than the disturbances that must be suppressed, in this frequency bandwidth.

2. It is important that the servo system does not make things much worse in frequency bandwidth of interest for detection of gravity wave signal. Since the sensor noise is much larger in this region it could reduce the good performance of the pendulum.

3. An additional criterion is that the open loop gain should be substantially less than one at frequency at which its phase is equal -180^0 i. e. system must be stable with appropriate gain and phase margins.

2.1 GENERAL DESCRIPTION OF THE 40 M SUSPENSION CONTROL SYSTEM

A schematic diagram of the control system of the 40m test mass suspension is shown in Fig. 2.1. The motion of the test mass is detected by a shadow sensor which consists of an LED - photodiode pair [3]. This signal is filtered and amplified by the suspension control electronics and fed back to the magnet-coil actuator to damp the test mass. Alternatively, a signal from an optical lever sensor or from the interferometer wavefront sensing system can be used; however, these are typically used only to provide a DC bias to the test mass orientation. An interferometer LSC (Length Sensing and Control) signal can be injected in the control loop.
The sensor/actuator head consists of a pair of an LED and a photodiode, a coil and a housing. Five sensor/actuator heads are supported by the head holders which are mounted on the suspension support structure, so that each head is located properly, along the corresponding magnet/standoff assembly: four heads on back and one sensor/actuator head on one side. They are designated as UL (Upper Left), UR (Upper Right), LL (Lower Left), LR (Lower Right) and SIDE. The LED-photodiode system senses the shadow of the magnet, thus position of the test

mass is detected. The current in the coil produces a Lorentz force on the magnet attached to the test mass. The system is illustrated in Fig. 2.2.

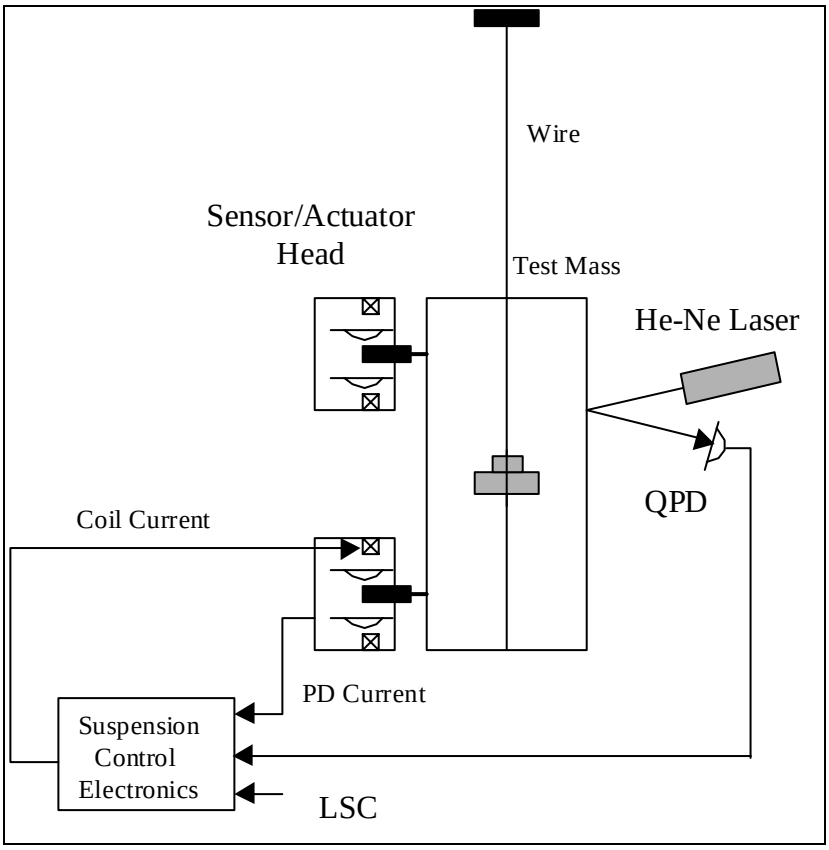

Figure 2.1 Schematic diagram of the control system for the 40m TM suspension

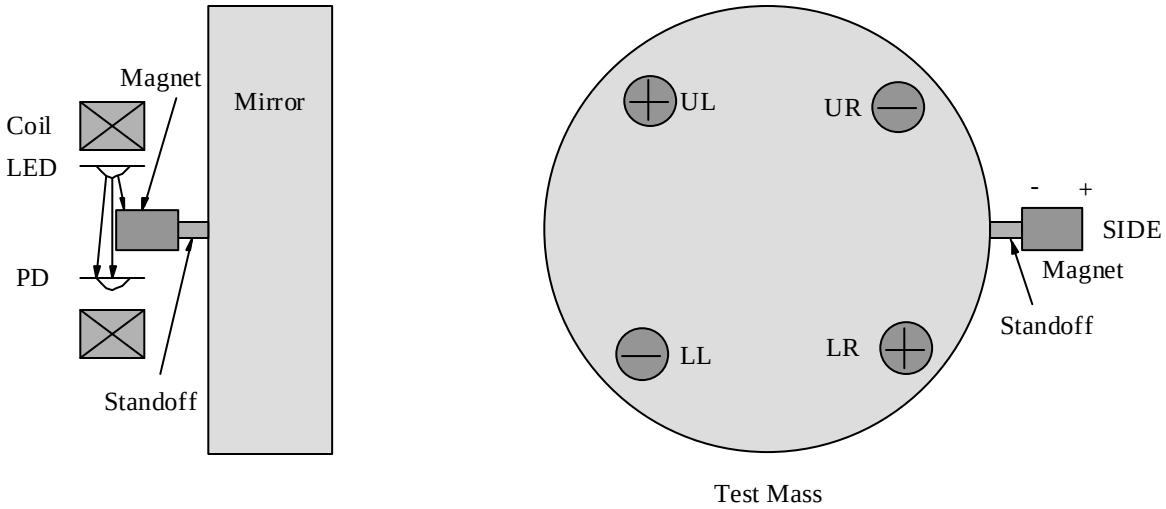

Figure 2.2 Sensor/Actuator heads and their position

The schematic diagram of the *electronic system of the suspension control* is shown in Fig. 2.3. *The suspension satellite detector/amplifier* provides current to the LEDs and converts photocurrent in the photodiode into voltage. The output of the suspension satellite detector/amplifier is then sent to *the suspension controller*. The signals that represent the position of each magnet are, by *the input matrix*, converted into position, pitch, yaw and side signal of the

test mass. The derivative of the signals is produced for damping, and amplified. *Coarse bias* (inside the suspension controller) and *WFS* (Wavefront sensing) are added to the pitch and yaw signals. Test signals can be also added to each signal. The signals are then, by the *output matrix*, converted into signals that are used for each *coil*. The signals are low pass filtered in order to reject sensor noise at higher frequencies, where the control is not active. The LSC signal may be added. *Drivers* inject currents into each coil, proportional to the control signal. The switch between the input matrix and the filter gain makes it possible to choose either the suspension's sensor signal or the 40m optical lever signal.

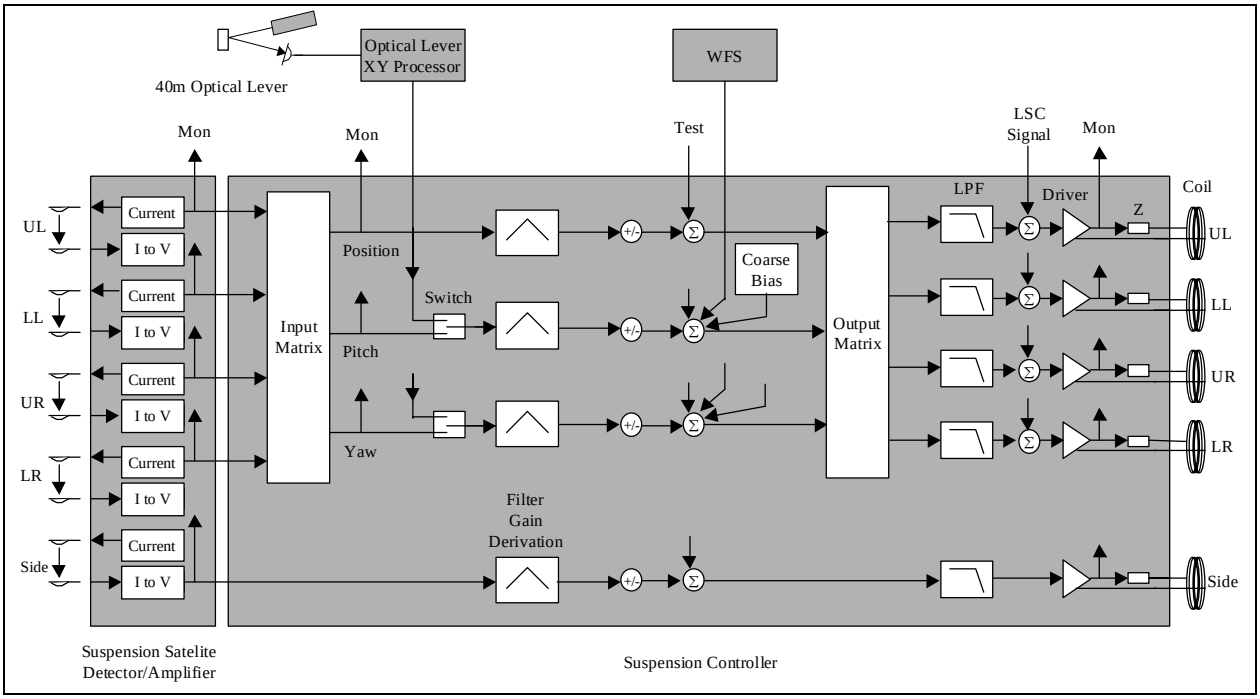

Figure 2.3 Schematic diagram of the electronic system of the suspension control

The sensor voltage from each sensor, $V_{S;UL/LL/UR/LR}$, is related to the sensor voltage for each degree of freedom, $V_{S;position/pitch/yaw}$, by an *input matrix* $\lfloor M_{S;i,j} \rfloor$ which is nominally unity and adjustable around unity

$$\begin{bmatrix} V_{S;position} \\ V_{S;pitch} \\ V_{S;yaw} \end{bmatrix} = \begin{bmatrix} M_{S;position,UL} & M_{S;position,LL} & M_{S;position,UR} & M_{S;position,LR} \\ M_{S;pitch,UL} & -M_{S;pitch,LL} & M_{S;pitch,UR} & -M_{S;pitch,LR} \\ M_{S;yaw,UL} & M_{S;yaw,LL} & -M_{S;yaw,UR} & -M_{S;yaw,LR} \end{bmatrix} \begin{bmatrix} V_{S;UL} \\ V_{S;LL} \\ V_{S;UR} \\ V_{S;LR} \end{bmatrix} \quad (2\text{-}2)$$

For example, the sensor voltage position signal is proportional to the sum of the sensor voltage from each sensor (UL, LL, UR, LR); the sensor voltage pitch signal is proportional to the difference between the sum of the upper and the sum of the lower sensor voltage signals, and the sensor voltage yaw signal is proportional to the difference between the sum of the left and the sum of the right sensor voltage signals.

The feedback voltage for each degree of freedom, $V_{F;position/pitch/yaw}$, is related to the feedback voltage to each actuator, $V_{F;UL/LL/UR/LR}$, by the *output matrix* $\lfloor M_{F;i,j} \rfloor$, which is nominally unity and adjustable around unity.

$$\begin{bmatrix} V_{F;UL} \\ V_{F;LL} \\ V_{F;UR} \\ V_{F;LR} \end{bmatrix} = \begin{bmatrix} M_{F;UL,position} & M_{F;UL.pitch} & M_{F;UL,yaw} \\ M_{F;LL,position} & -M_{F;LL.pitch} & M_{F;LL,yaw} \\ M_{F;UR,position} & M_{F;UR.pitch} & -M_{F;UR,yaw} \\ M_{F;LR,position} & -M_{F;LR.pitch} & -M_{F;LR,yaw} \end{bmatrix} \begin{bmatrix} V_{F;position} \\ V_{F;pitch} \\ V_{F;yaw} \end{bmatrix} \qquad (2\text{-}3)$$

A current-source type driver is used for driving a the coil. As shown in Fig. 2.4, the coil is placed inside the feedback loop of the driver operational amplifier. The LSC signal is injected into the inverting input of the operational amplifier. The voltage at the right end of the series resistor (R_3) can be monitored as the LSC feedback signal. R_3 can be a smaller resistance during the lock acqusition and switched to a larger resistance for signal monitoring. The LSC input can be disabled by a switch. The designers point out the following advantages of this configuration:

- Because of the high impedance looking from the coil, no pick-up current can flow in the coil.
- The Monitor signal is free from any pick-up existing in the long loop containing the coil.
- Because of the high impedance looking from the coil, the vibration of the coil with respect to the magnet doesn't cause eddy currents; the mass is not dragged.
- The maximum current for the LSC signal can be big enough with a smaller value of R_3 for the acquisition mode.
- The signal to noise ratio at the monitor point can be good enough with a greater value of R_3 for the operational mode.
- Switching between the acquisition mode and the operation mode doesn't change the gain of both the LSC system and the damping control system.
- The Effect of any noise produced before the summing junction, including the Johnson noise of R_1 and R_2, is suppressed by the loop gain of the LSC servo system

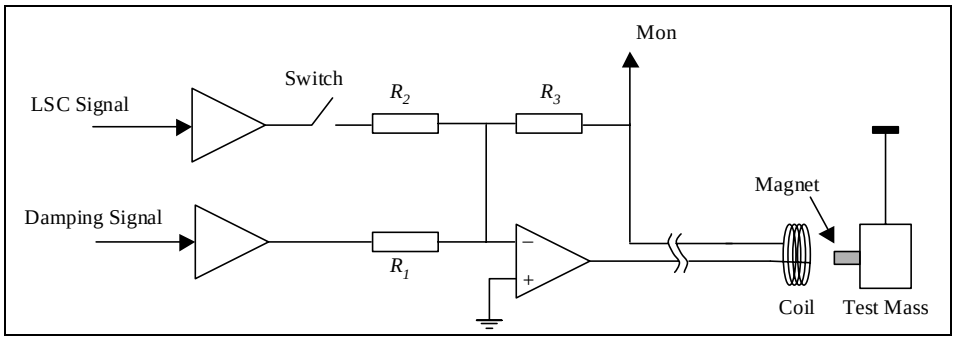

Figure 2.4 Schematic diagram of the output driver and the LSC signal injection

The Magnetic field around a magnet has, due to the finite dimensions of the magnet, a radial component (Fig. 2.5) which will cause a force acting on a coil in horizontal direction (z) when current flows through the coil. According to Newton's Third Law of motion, the same force but in opposite direction is acting on the magnet, and thus the test mass. If we assume that radial component of magnetic field B_r is constant in every point of the coil, then the intensity of a horizontal force acting on the coil, that is, on the magnet, will be given by

$$F = \int_l IBdl = IB \cdot N \cdot \pi d = const \cdot I \,, \quad (2\text{-}4)$$

where N is number of turns of the coil, d is diameter of the coil and I is the current applied to the coil.

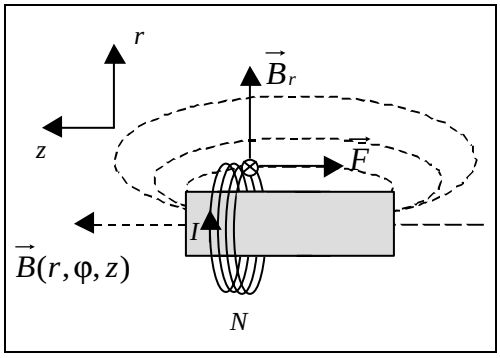

Figure 2.5 Horizontal force acting on the coil

If V_d is the voltage damping signal, then from Fig. 2.4 it can be easily seen that the current applied to the coil is related to this voltage as follows

$$I = \frac{V_d}{R_1}. \qquad (2\text{-}5)$$

2.2 BLOCK DIAGRAM OF CONTROL SYSTEM

Fig. 2.6 shows [3] a block diagram of the 40m suspension damping control system for each degree of freedom. Force (or torque) applied to the test mass produces displacement (or angle) of the test mass by the transfer function which has two almost imaginary poles at the resonance frequency. The displacement (or angle) is then detected by the sensor, producing current with a frequency-independent coefficient. The voltage signal is then filtered/amplified by a transfer function of the electronics, which consists of a zero at a DC (from the real differentiator – in order to sense velocity of the mirror) and 10 pole Chebyshev (1 dB ripple) 12 Hz low-pass filter (so that sensor noise, which is dominant at high frequencies, can be successfully suppressed). This feedback current produces a force (or torque) with a frequency independent coefficient of the actuator. The sensor noise is injected before the sensor transfer function. This noise is suppressed by the low pass filter of the electronics. The driver noise is, on the other hand, injected after the filter.

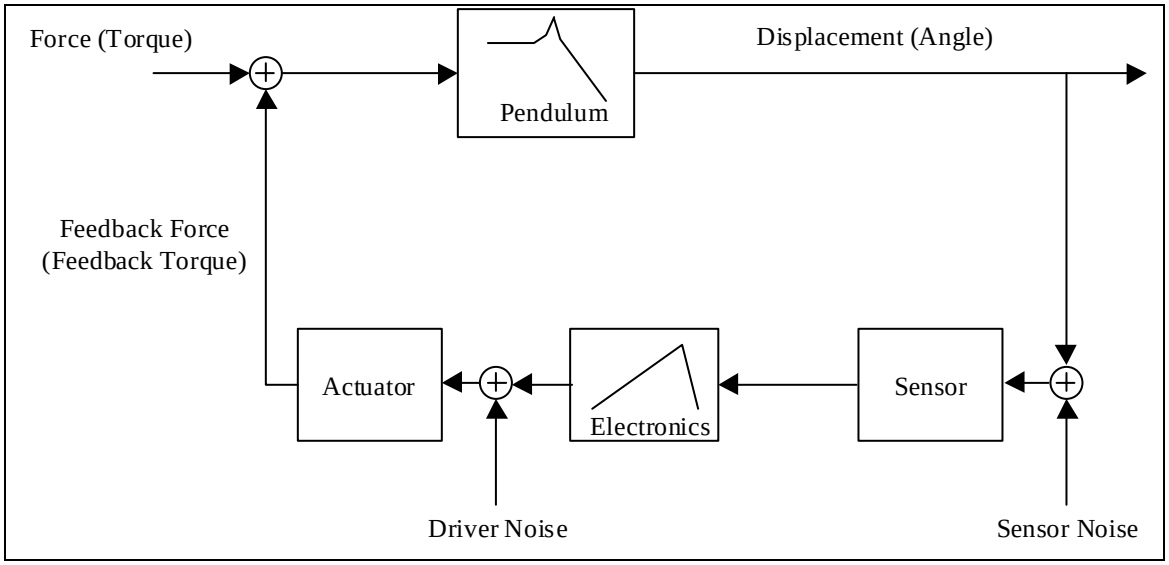

Figure 2.6 Block diagam of the 40m suspension damping control system together with typical noise sources

A. SENSOR AND ACTUATOR

The Sensor parameters are[3]

- LED current: 10 mA
- Reverse PD voltage: 10 V
- PD current-voltage converting resistance: 20 kΩ
- Sensitivity: 35 μA per head
- Sensor noise: 9.4×10^{-11} m/$\sqrt{\text{Hz}}$

Actuator parameters

- Current-force coefficient: approximately 21 mN/A
- Driver noise: 2.0×10^{-11} A/$\sqrt{\text{Hz}}$
- $R_1 = 1\,\text{k}\Omega,\ R_2 = 100\,\Omega,\ R_3 = 100\,\Omega$ (acquisition mode), $1\,\text{k}\Omega$ (operational mode)

B. GAIN OF CONTROL SYSTEM

The loop gain is set to give pseudo-critical damping, which is defined [3] as a damping with a minimum gain which makes the closed loop transfer function in gain bumpless around the resonance frequency. The pseudo-critical damping is accomplished when the open loop gain around the resonance frequency is approximately unity:

[Pendulum(@DC)] ×[Sensor] × [Electronics(@f_0)] × [Actuator] = 1.

The Pendulum gain at DC for all degrees of freedom can be obtained from (1-12c), (1-16a) and (1-16b). For the position degree of freedom (T = 0, s = 0) we obtain

$$\left(\frac{x}{F}\right)_{DC} = \frac{d + d_p}{Mg}. \qquad \text{(2-6a)}$$

The DC gain for the pitch degree of fredom (F = 0, s = 0) is given by

$$\left(\frac{\theta}{T}\right)_{DC} = \frac{1}{Mgd_p}, \qquad \text{(2-6b)}$$

and for the yaw degree of freedom, we have

$$\left(\frac{\varphi}{T}\right)_{DC} = \frac{4d}{MgDd_y}. \qquad \text{(2-6c)}$$

Since the sensor sensitivity per head is 35 μA/mm, and there are four heads on the back of the mirror, the sensitivity for position degree of freedom is 4×35 μA/mm = 0.14 A/m. The Actuator's current to force coefficient is 21 mN/A, so the current to force coefficient for the position degree of freedom will be 4×21 mN/A = 8.4×10^{-2} N/A . The Sensor sensitivity and current to torque coefficient for the pitch and yaw degrees of freedom is obtained by multiplying the sensitivity and current to force coefficient for the position degree of freedom with the conversion coefficient 0.032 rad/m. We have only one sensor/actuator head for the side degree of freedom, so all parameters are 4 times smaller compared with parameters for position degree of freedom. Table 2.1 summarizes the gain of each block in Fig 2.6 for pseudo-critical damping for each degree of freedom.

Degree of Freedom	**Pendulum at DC**	**Sensor**	**Electronics at f_0**	**Actuator**
Position	2.24×10^{-2} m/N	0.14	3.9×10^{3}	8.4×10^{-2} N/A
Side	2.24×10^{-2} m/N	3.5×10^{-2} A/m	6.2×10^{4}	2.1×10^{-2} N/A

Pitch	48 rad/Nm	4.5×10^{-3} A/rad	1.7×10^{3}	2.7×10^{-3} Nm/A
Yaw	34 rad/Nm	4.5×10^{-3} A/rad	2.4×10^{3}	2.7×10^{-3} Nm/A

Table 2.1 Gains of control system for each degree of freedom

C. SENSOR NOISE

The sensor noise is dominated by the shot noise at the photodiode. It is attenuated by the steep low pass filter. Table 2.2 shows resultant displacement noise at 40 Hz caused by the sensor noise, together with sensor noise, loop gain and coupling coefficient [3]. The mirror displacement noise caused by sensor noise is given by

[Displacement Noise] = [Effective Sensor Noise] × [Loop Gain] × [Coupling].

Degree of Freedom	Effective Sensor Noise at 40 Hz	Open Loop Gain at 40 Hz	Coupling	Displacement Noise at 40 Hz
Position	4.7×10^{-11} m/$\sqrt{\text{Hz}}$	7×10^{-10}	1	4×10^{-20} m/$\sqrt{\text{Hz}}$
Side	9.4×10^{-11} m/$\sqrt{\text{Hz}}$	7×10^{-10}	< 0.1	$< 7\times10^{-21}$ m/$\sqrt{\text{Hz}}$
Pitch	1.5×10^{-9} rad/$\sqrt{\text{Hz}}$	4×10^{-10}	< 3 mm	$< 2\times10^{-21}$ m/$\sqrt{\text{Hz}}$
Yaw	1.5×10^{-9} rad/$\sqrt{\text{Hz}}$	4×10^{-10}	< 3 mm	$< 2\times10^{-21}$ m/$\sqrt{\text{Hz}}$

Table 2.2 Sensor noise and the resultant displacement noise for each degree of freedom

D. DRIVER NOISE

The driver noise is produced after the steep low pass filter [3]. This includes the Johnson noise of the series impedance R_3. Table 2.3 summarizes the displacement noise caused by the driver noise for each degree of freedom.

[Displacement Noise] = [Effective Driver Noise] ×[Actuator] ×[Pendulum] ×[Coupling].

Degree of Freedom	Effective Driver Noise at 100 Hz	Actuator	Pendulum at 100 Hz	Coupling	Displacement Noise at 100 Hz
Position	$1.\times10^{-11}$ A/$\sqrt{\text{Hz}}$	8.4×10^{-2} N/A	1.6×10^{-6} m/N	1	1.3×10^{-18} m/$\sqrt{\text{Hz}}$
Side	2.0×10^{-11} A/$\sqrt{\text{Hz}}$	2.1×10^{-2} N/A	1.6×10^{-6} m/N	< 0.1	$< 6.7\times10^{-20}$ m/$\sqrt{\text{Hz}}$
Pitch	1.0×10^{-11} A/$\sqrt{\text{Hz}}$	2.7×10^{-3} Nm/A	1.2×10^{-3} rad/Nm	< 3 mm	$< 9.7\times10^{-20}$ m/$\sqrt{\text{Hz}}$
Yaw	1.0×10^{-11} A/$\sqrt{\text{Hz}}$	2.7×10^{-3} Nm/A	1.2×10^{-3} rad/Nm	< 3 mm	$< 9.7\times10^{-20}$ m/$\sqrt{\text{Hz}}$

Table 2.3 Driver noise and the resultant displacement noise for each degree of freedom

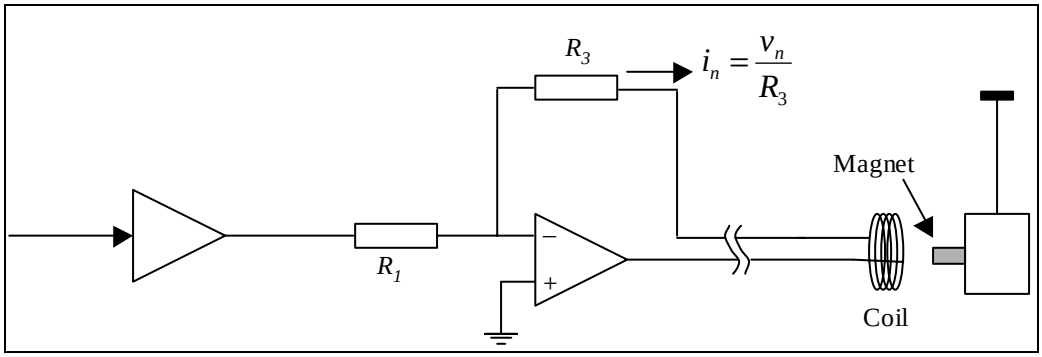

Figure 2.7 The driver noise injection

If we use greater series impedance R_3, the injected current noise into the coil will be smaller. On the other hand, we'll have a small control current so the dynamic range of the control system will be reduced.

E. RANGE OF ACTUATOR

The range of the actuator for each degree of freedom is summarized in Table 2.4 [3].

[Range] = [Maximum Driver Current] ×[Actuator] ×[Pendulum]

Degree of Freedom	Maximum Driver Current	Actuator	Pendulum at DC	Range at DC
Position	2.4×10^{-2} A_{pp}	8.4×10^{-2} N/A	2.24×10^{-2} m/N	4.4×10^{-5} m_{pp}
Side	2.4×10^{-2} A_{pp}	2.1×10^{-2} N/A	2.24×10^{-2} m/N	1.1×10^{-5} m_{pp}
Pitch	2.4×10^{-2} A_{pp}	2.7×10^{-3} Nm/A	48 rad/Nm	3.1×10^{-3} rad_{pp}
Yaw	2.4×10^{-2} A_{pp}	2.7×10^{-3} Nm/A	34 rad/Nm	2.2×10^{-3} rad_{pp}

Table 2.4 Range of actuator for each degree of freedom

3. SIMULINK MODELING OF THE 40 M PENDULUM CONTROL SYSTEM

3.1 POSITION AND PITCH DEGREES OF FREEDOM

In Fig. 3.1(a,b,c) the Simulink model of the 40m pendulum with velocity damping control for position and pitch degrees of freedom is shown. From the Bode diagrams it can be seen that with appropriate gain setting the transfer function becomes bumpless around the resonance frequency (Fig. 3.2(a,b)). In Fig. 3.3(a,b) the open loop transfer functions for position and pitch degrees of freedom are shown. We can see that the system is stable with appropriate gain and phase margins as indicated in these figures. In Fig. 3.4(a,b) the negative feedback loop transfer functions are shown. We have zero at zero, and 20 dB/dec for low frequencies in order to sense the velocity of the test mass. For frequencies that are above the Chebyshev low pass filter cut-off frequency (12 Hz) we have very steep roll-off with approximately -180 dB/dec in order to attenuate sensor noise, which is dominant at higher frequencies.

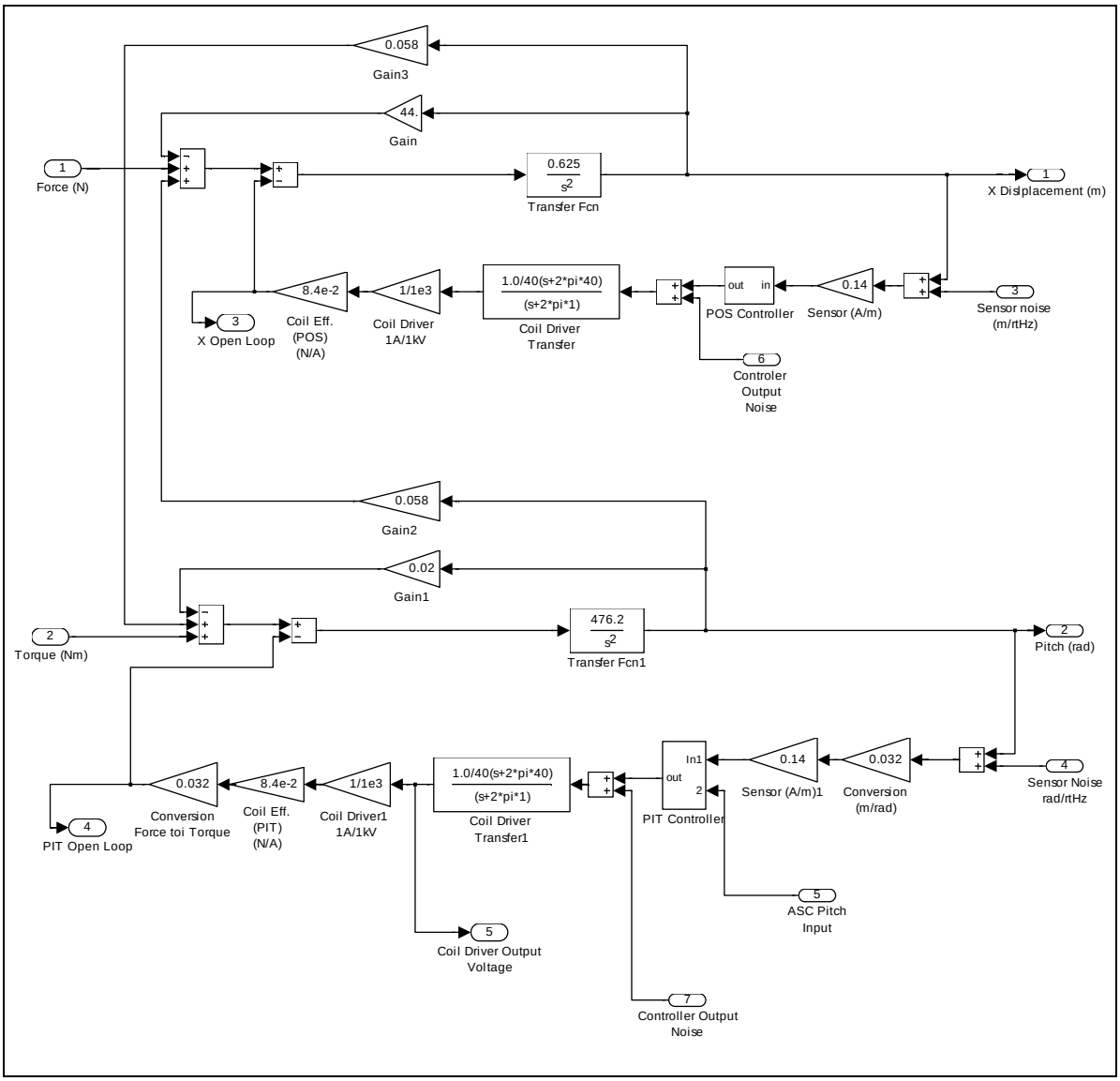

Figure 3.1(a) The Simulink model of the 40m pendulum with velocity damping for position and pitch degrees of freedom

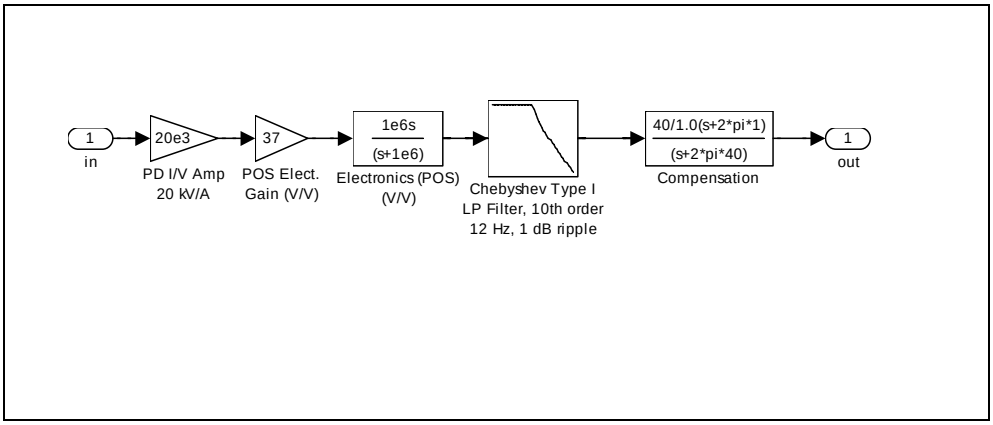

Figure 3.1(b) The Simulink model of the position controller

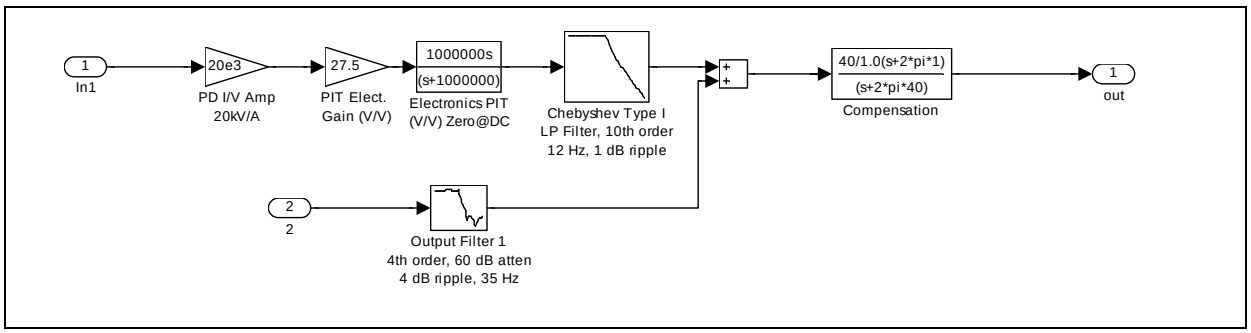

Figure 3.1(c) The Simulink model of the pitch controller

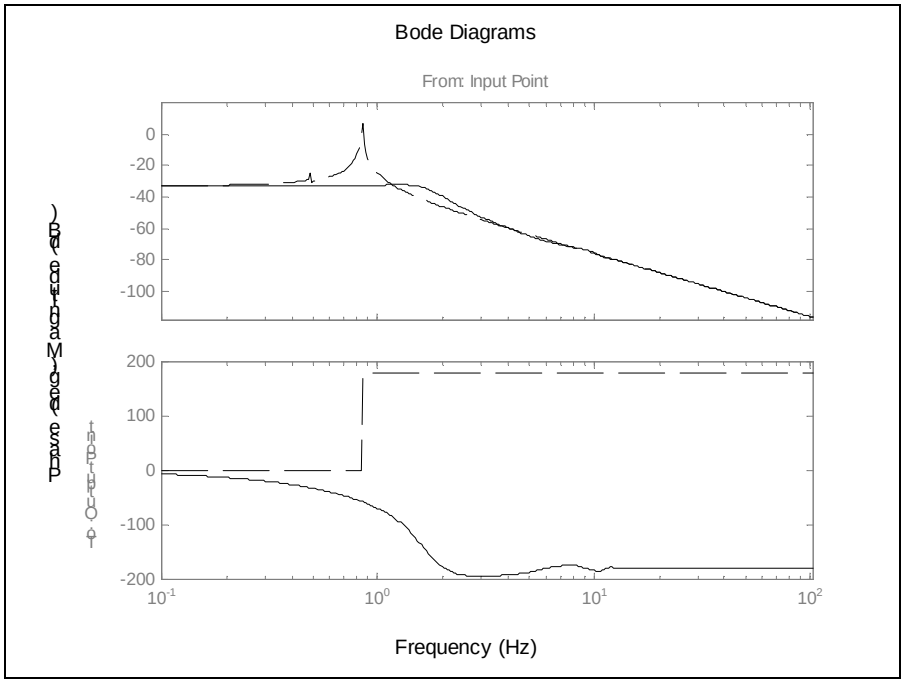

Figure 3.2(a) Bode diagrams of the "from force to position" transfer function with (solid) and without (dash) controllers

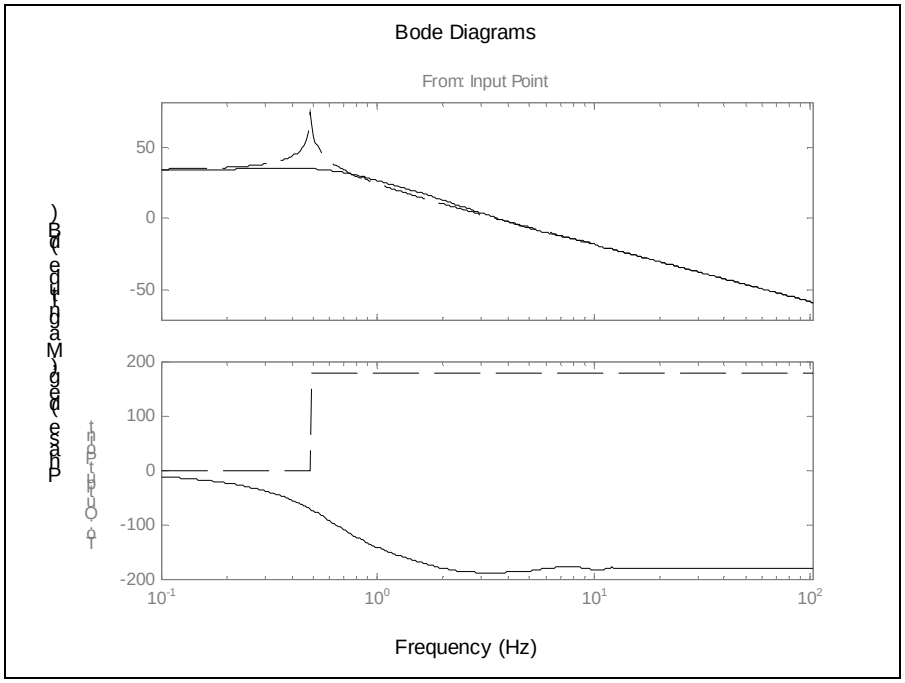

Figure 3.2(b) Bode diagrams of the "from torque to pitch" transfer function with (solid) and without (dash) controllers

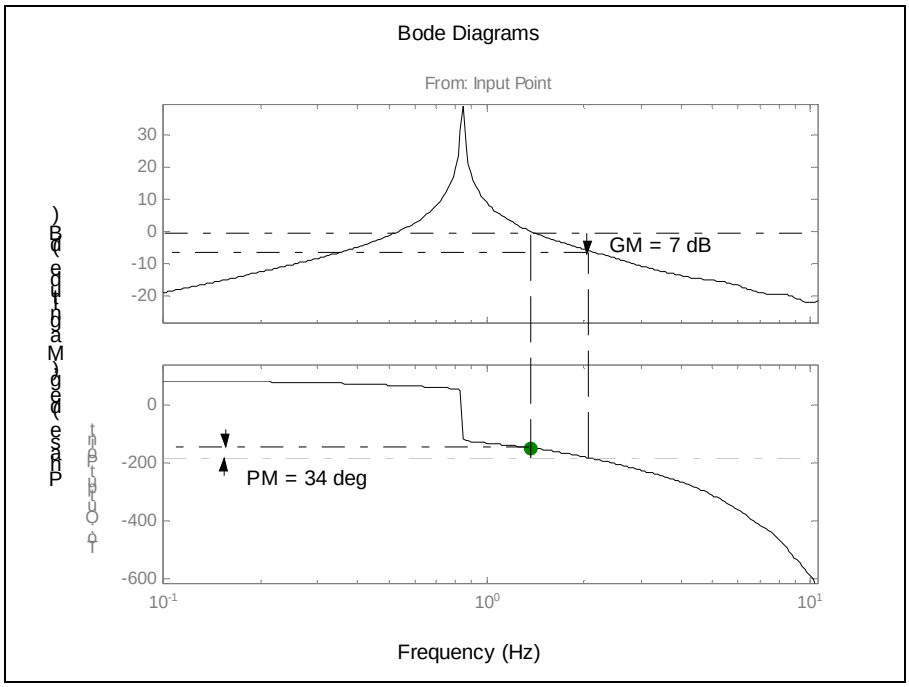

Figure 3.3(a) Bode diagrams of the position open loop transfer function showing stability

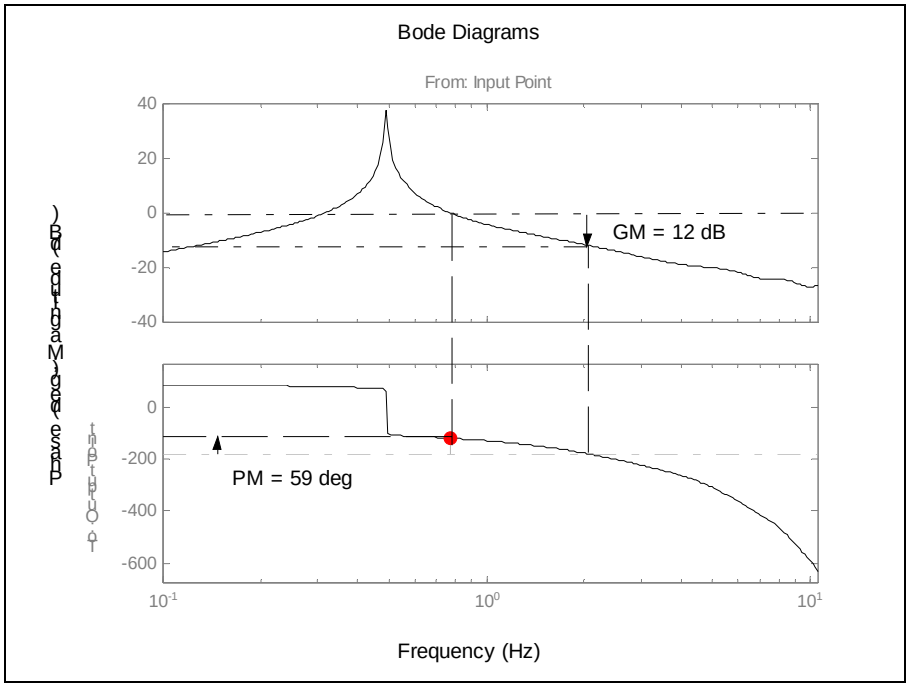

Figure 3.3(b) Bode diagrams of the pitch open loop transfer function showing stability

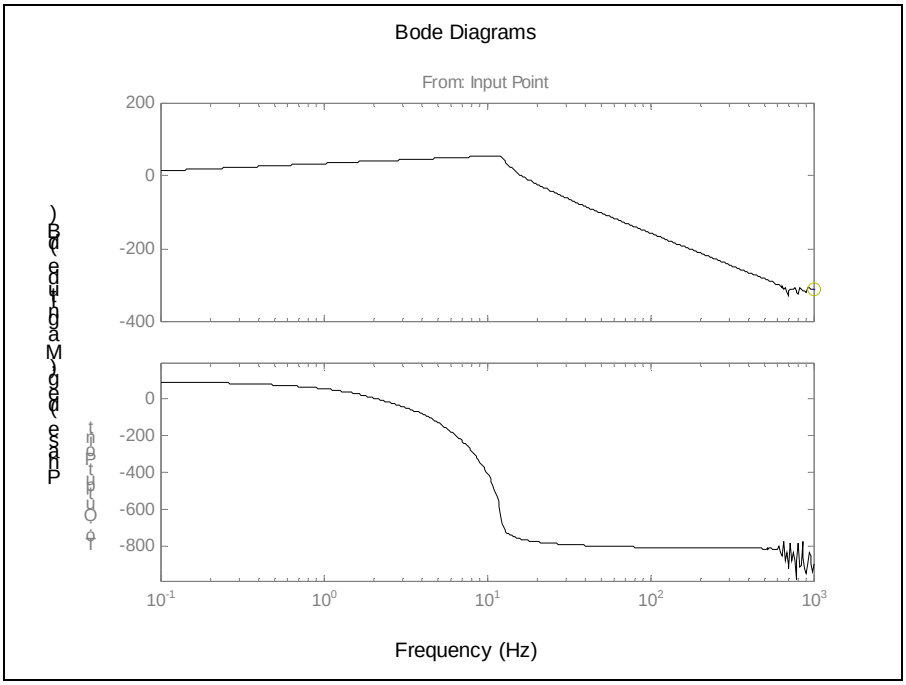

Figure 3.4(a) Bode diagrams of the position negative feedback transfer function

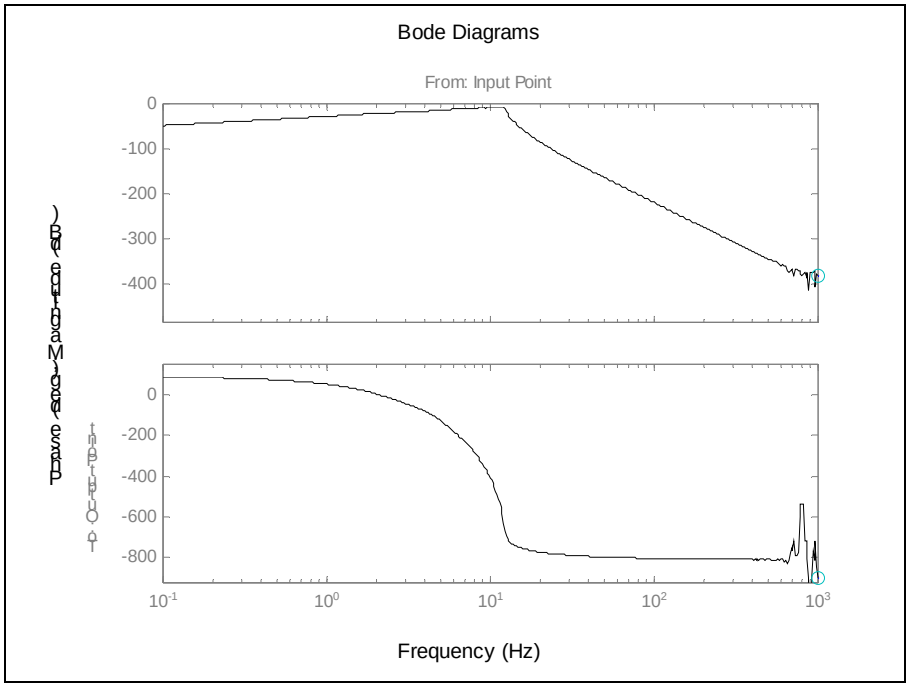

Figure 3.4(b) Bode diagrams of the pitch negative feedback transfer function

3.2 YAW DEGREE OF FREEDOM

In Fig. 3.5(a,b) the Simulink model of the 40m pendulum with velocity damping control for the yaw degree of freedom is shown. From the Bode diagrams it can be seen that with appropriate gain setting the transfer function becomes bumpless around the resonance frequency (Fig. 3.6). In Fig. 3.7 the open loop transfer functions for the yaw degree of freedom is shown. We can see that the system is stable with appropriate gain and phase margins as indicated in this figure. In Fig. 3.8 the negative feedback loop transfer function is shown.

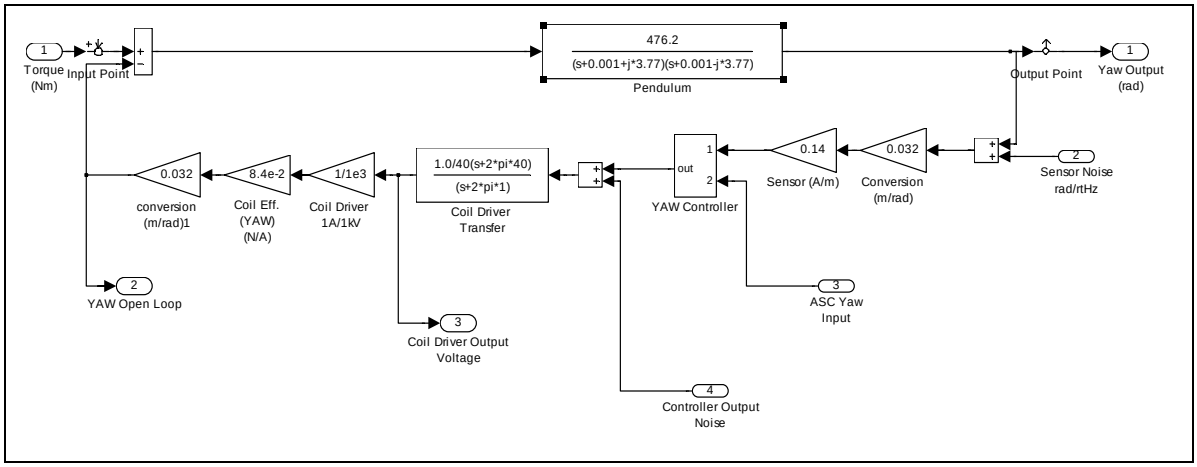

Figure 3.5(a) The Simulink model of the 40m pendulum with velocity damping for yaw degree of freedom

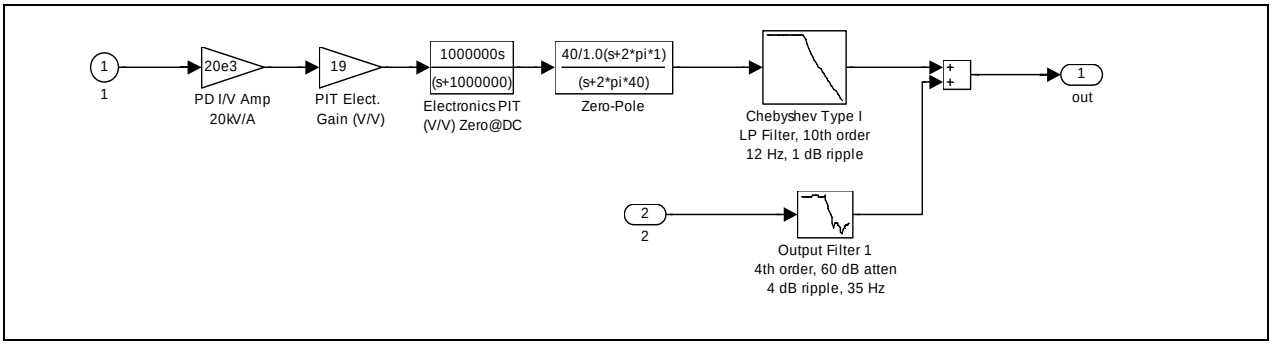

Figure 3.5(b) The Simulink model of the yaw controller

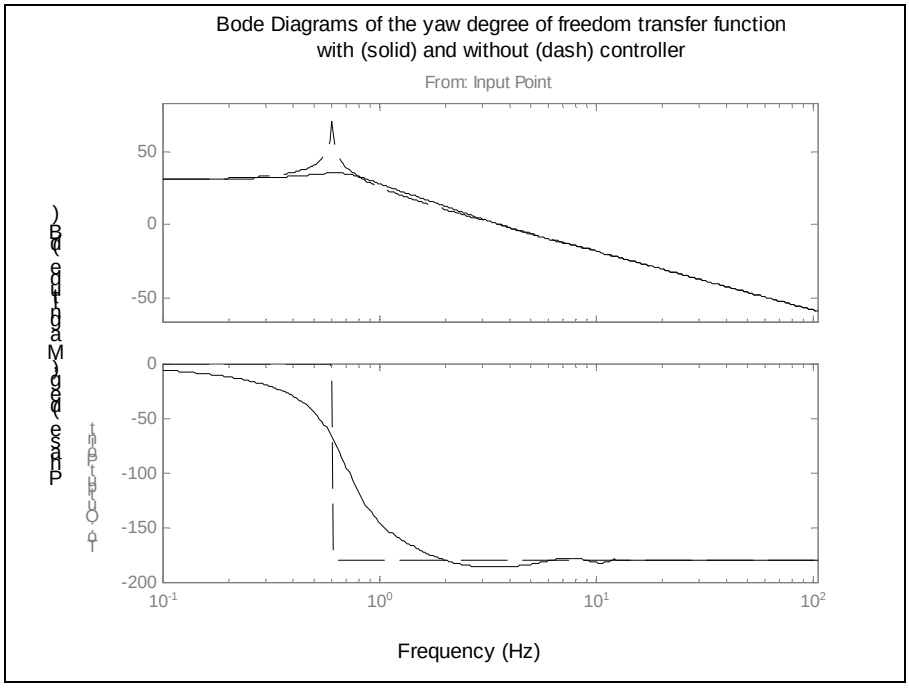

Figure 3.6 Bode diagrams of the "from torque to yaw" transfer function with (solid) and without (dash) controller

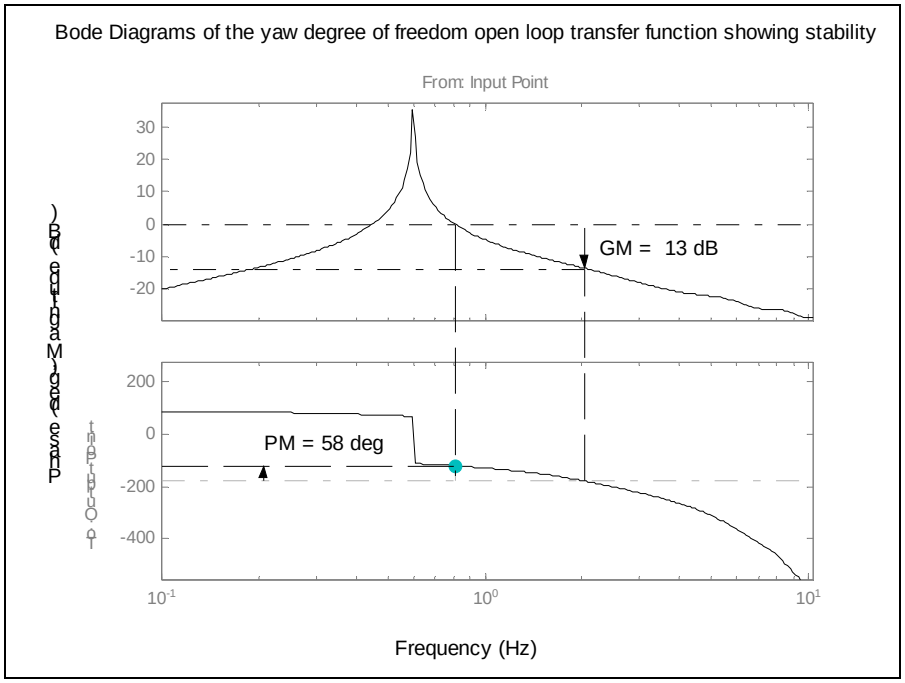

Figure 3.7 Bode diagrams of the yaw open loop transfer function showing stability

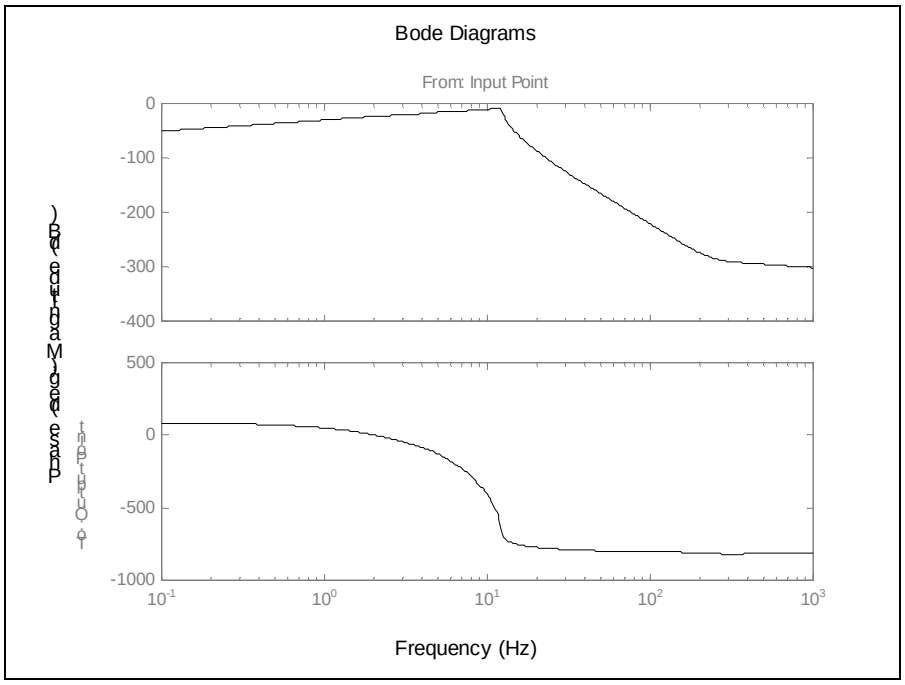

Figure 3.8 Bode diagrams of the yaw negative feedback transfer function

3.3 TIME RESPONSE

A Simulink model of the critically damped suspension Optics, giving the position and pitch motion of the pendulum system with horizontal motion of the suspension point, is shown in Fig. 3.9. We used recorded data of the horizontal ground motion. From the time response of designed system to low frequency ground motion (Fig. 3.10) it can be easily seen that the motion of the suspended test mass in accordance with the ground motion is as good as can be expected at lower frequencies. The reason for this lies in the fact that the sensor/actuator heads are fixed on the tower and they move together with suspension point. Therefore, this system brings to zero only relative motion of the suspended test mass (relative to the motion of the suspension point). However, in Fig. 3.11(a,b,c) the system's time response to higher frequency disturbances is shown. From these figures it can be seen that critically damped suspension optics successfully suppress high frequency component at 10 Hz without introducing oscillations at the pendulum frequency (Eq. (1-19)).

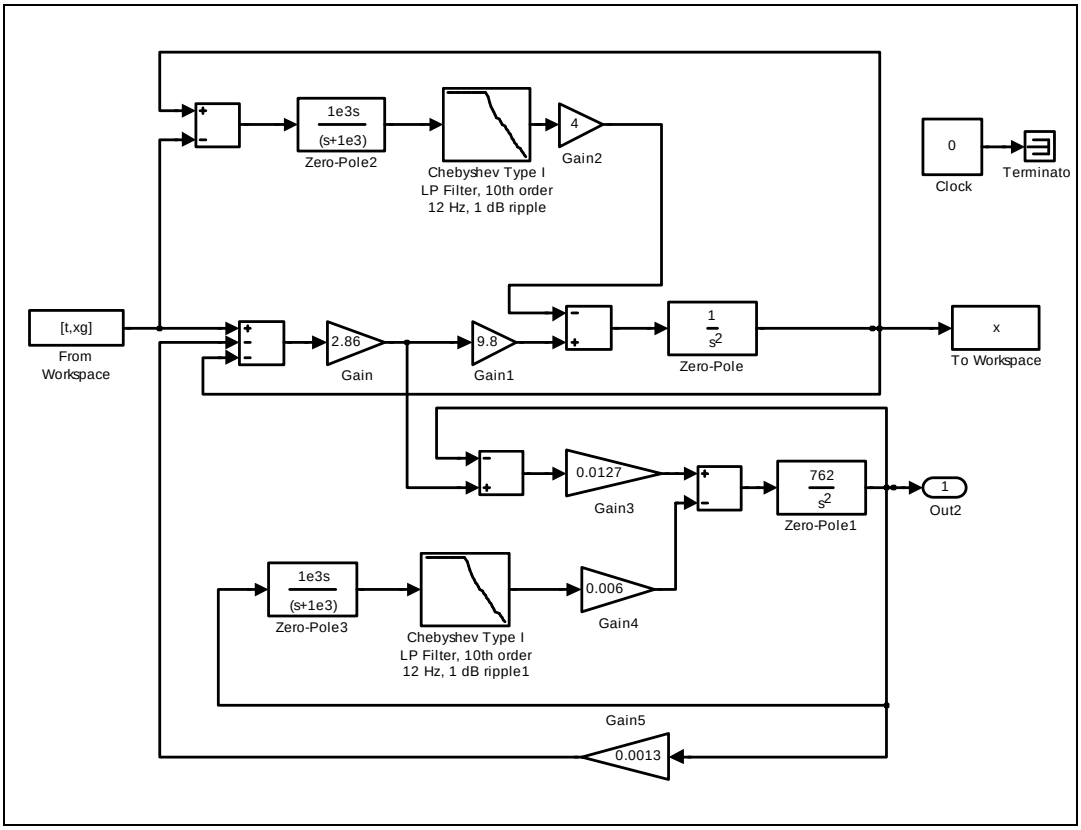

Figure 3.9 The time-domain Simulink model of critically damped suspension optics for position and pitch degrees of freedom

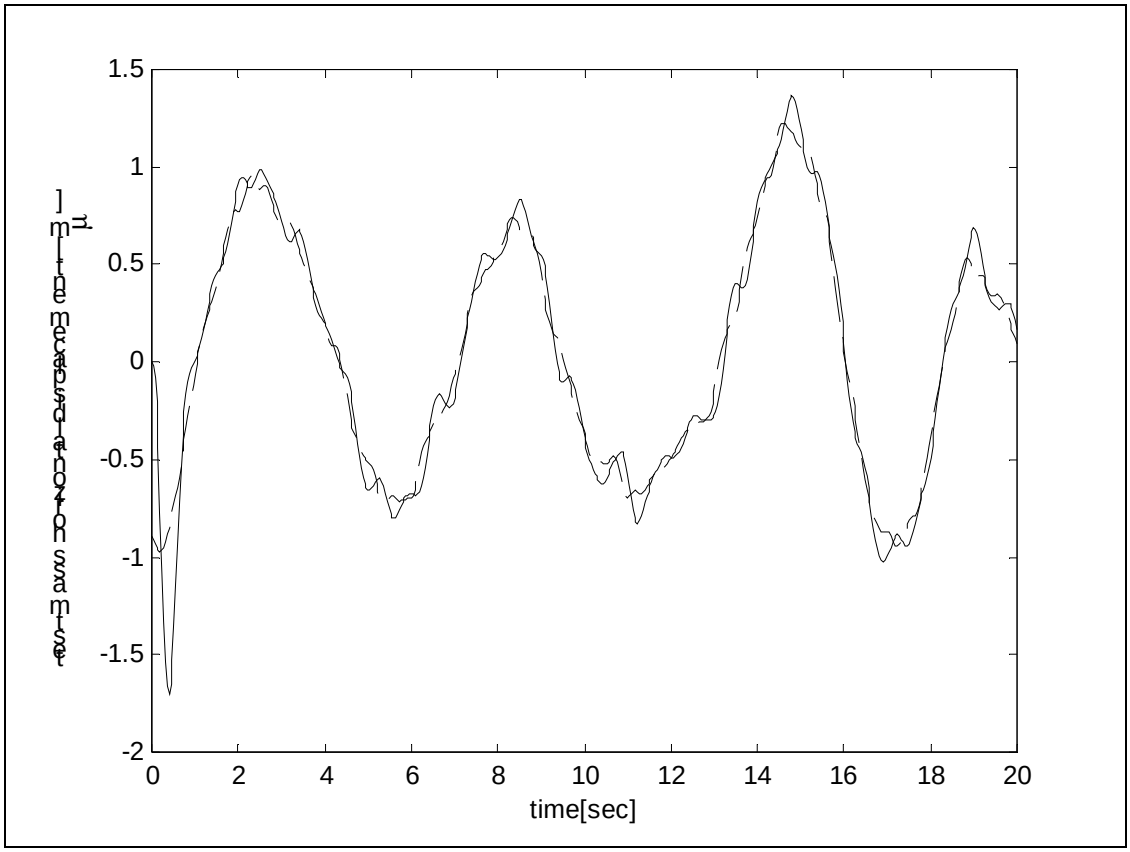

Figure 3.10 Critically damped suspension optics response (solid curve) to ground motion of the suspension point (dash curve).

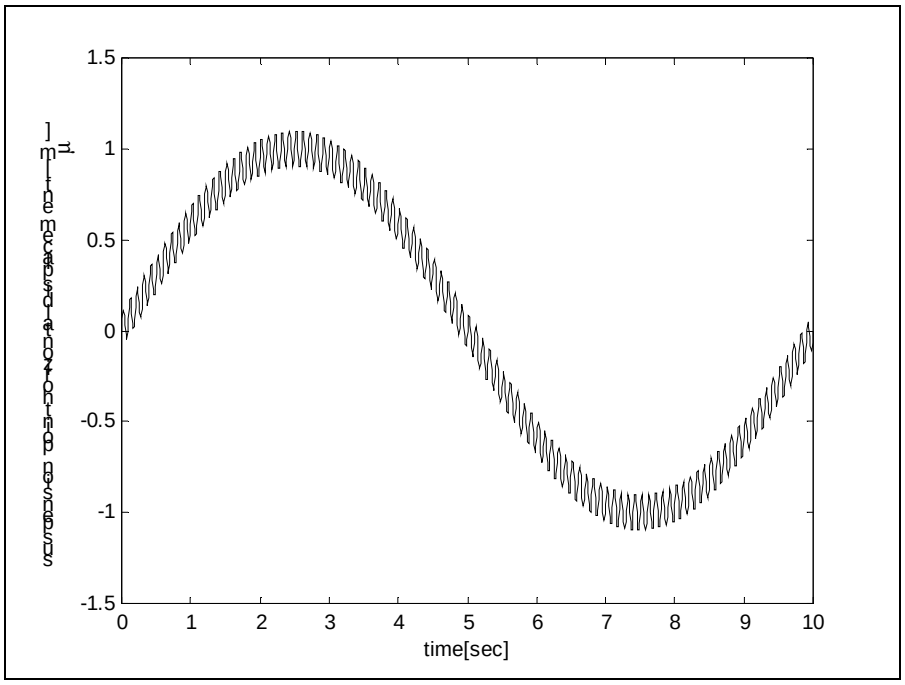

Figure 3. 11(a) The suspension point horizontal motion with a higher frequency component at 10 Hz.

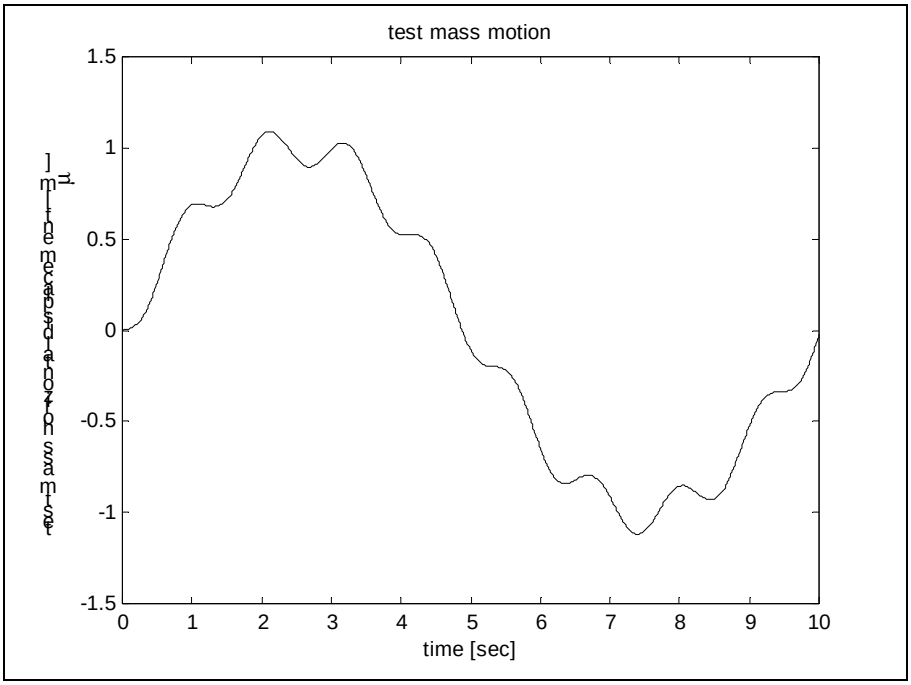

Figure 3.11(b) The pendulum response to suspension point motion.

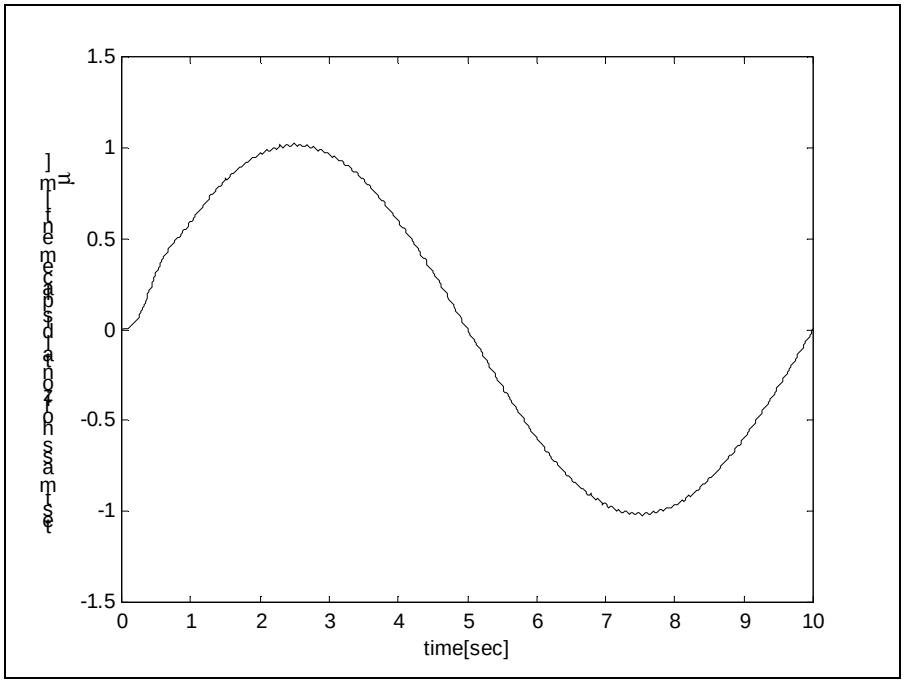

Figure 3.11(c) The critically damped suspension optics response to suspension point motion.

4. Simulink modeling of a Digital LOS and SOS Control System For Ligo

THIS SECTION COVERS THE DESIGN OF A DIGITAL LARGE OPTIC SUSPENSION (LOS) AND SMALL OPTIC SUSPENSION (SOS) CONTROL SYSTEM THAT CAN BE USED AS A REPLACEMENT FOR THE EXISTING LIGO LOS AND SOS CONTROLLERS [8].

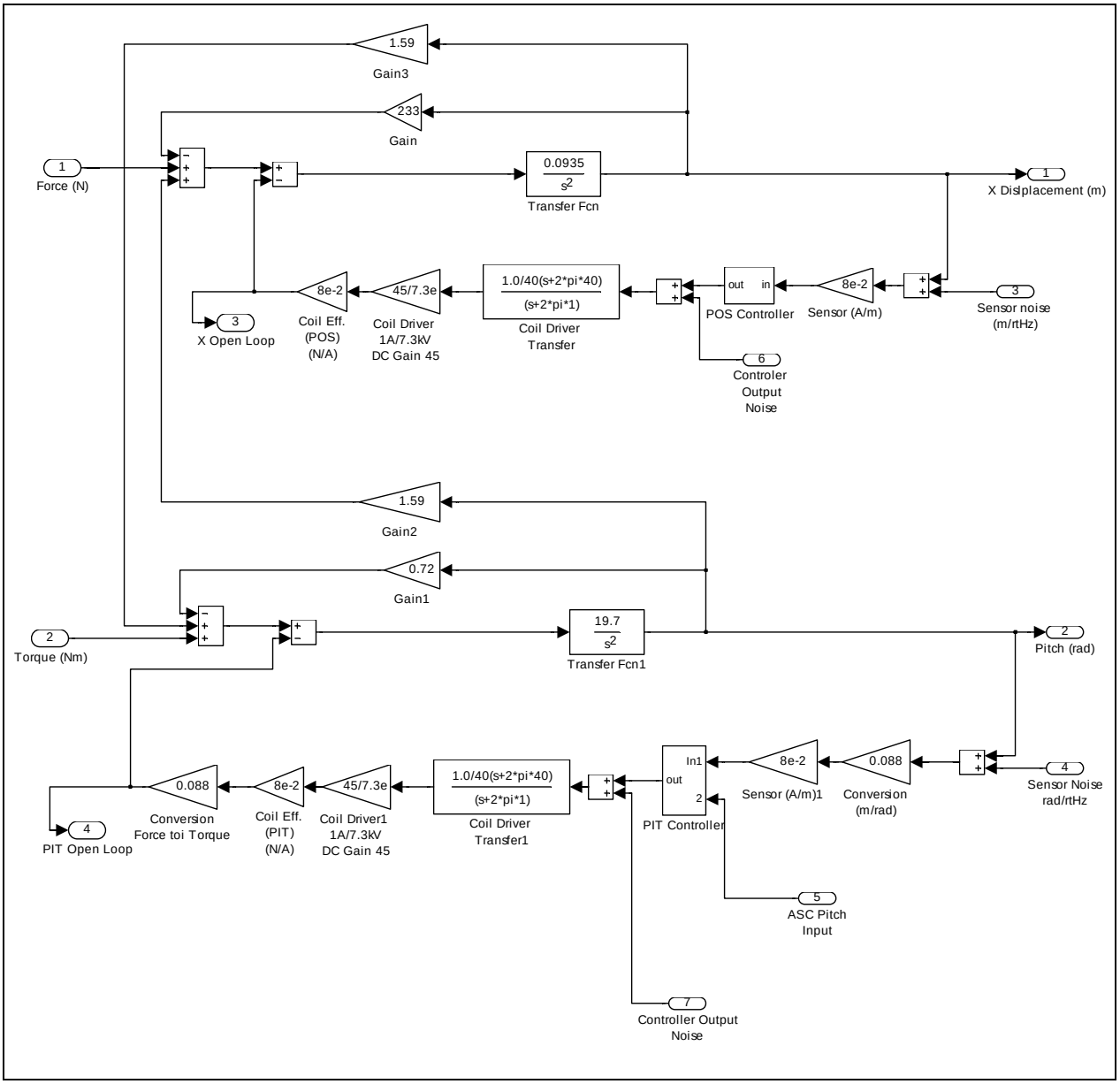

Figure 4.1 LOS Position and Pitch Servo Model

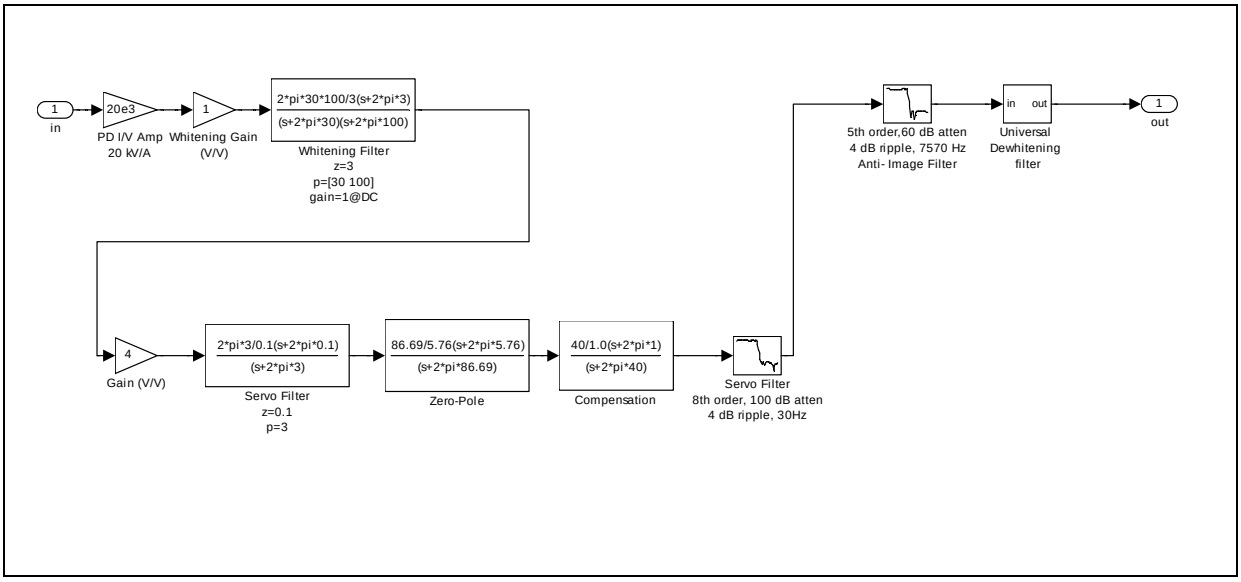

Figure 4.2 LOS Position Controller

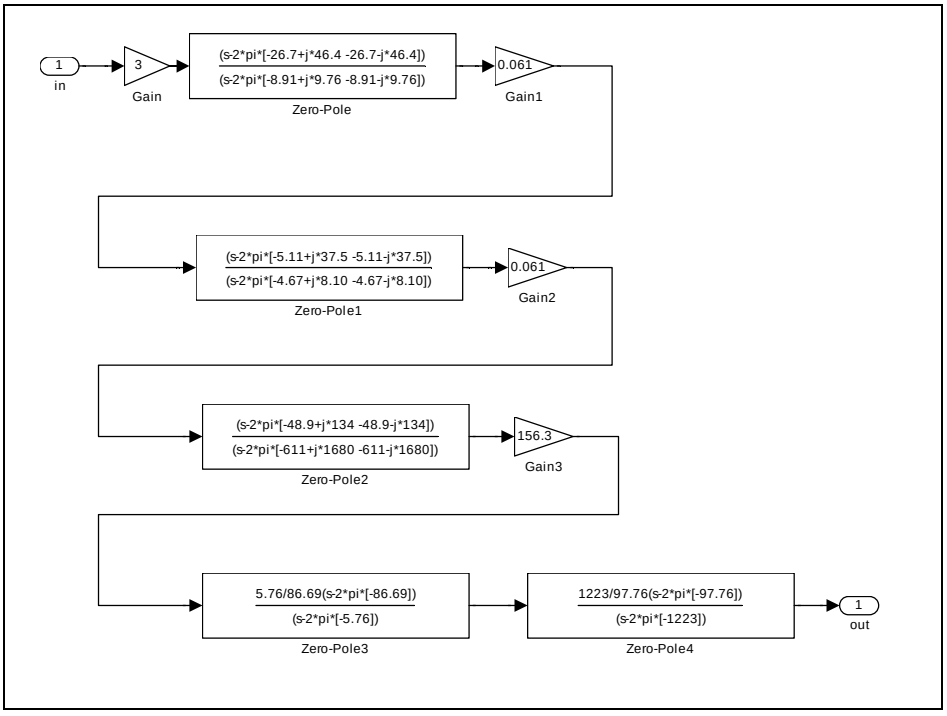

Figure 4.3 Universal Dewhitening Filter Used for Position, Pitch and Yaw Degrees of Freedom

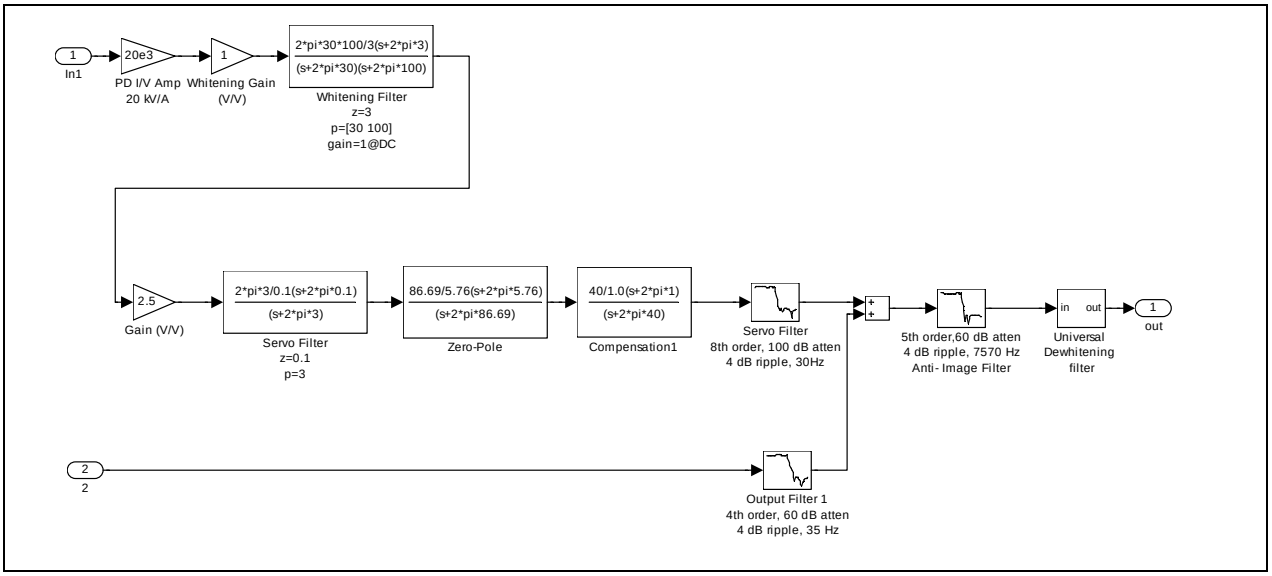

Figure 4.4 LOS Pitch Controller

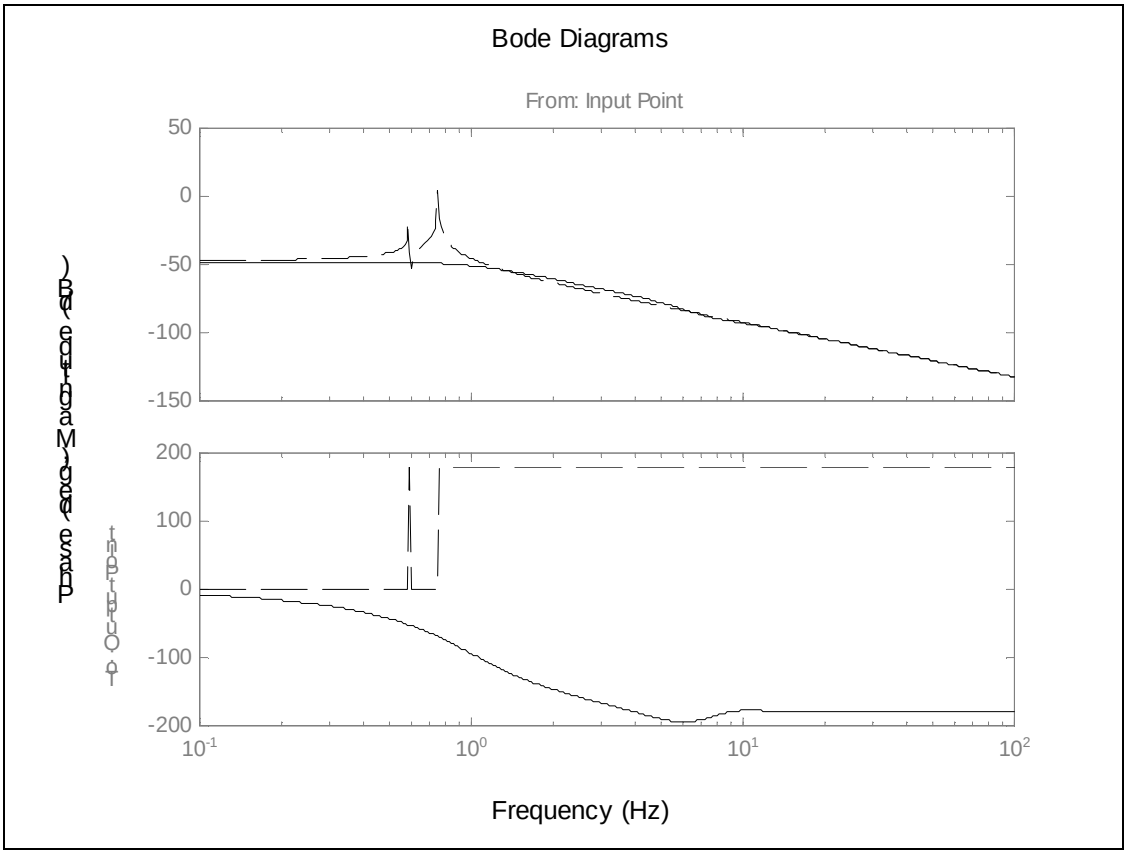

Figure 4.5 Bode Diagrams for Position Degree of Freedom with (solid) and without (dash) Controllers

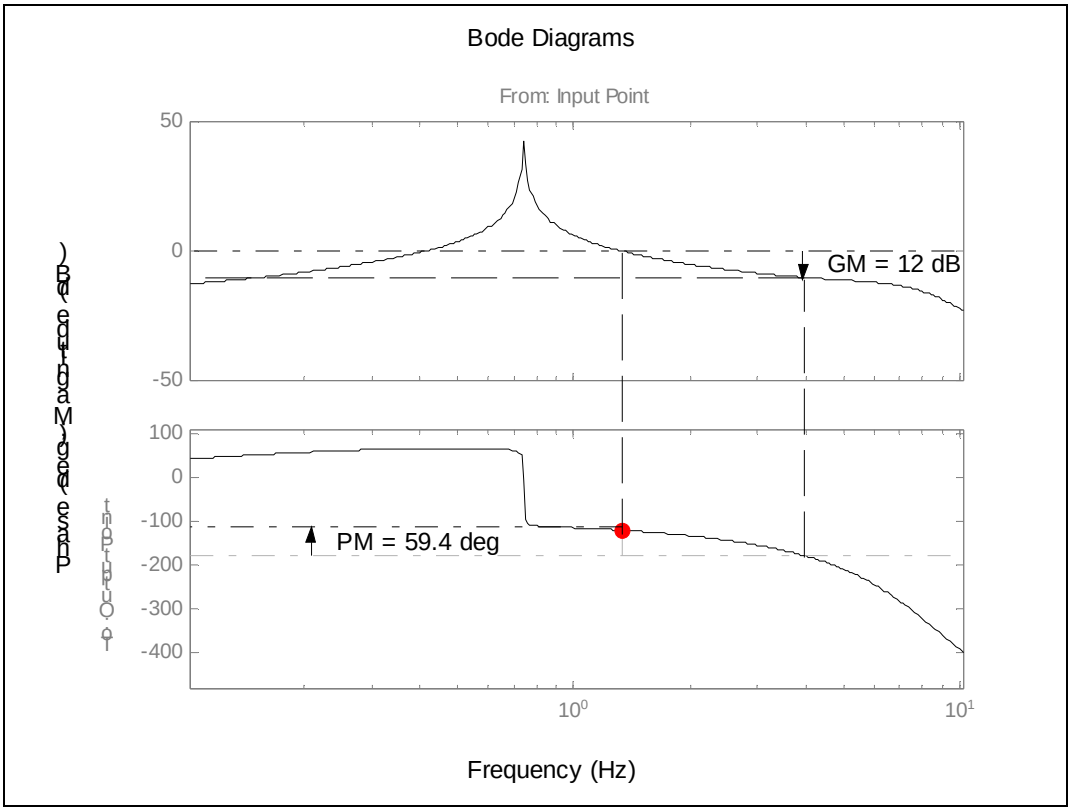

Figure 4.6 Bode diagrams for position open loop transfer function showing stability

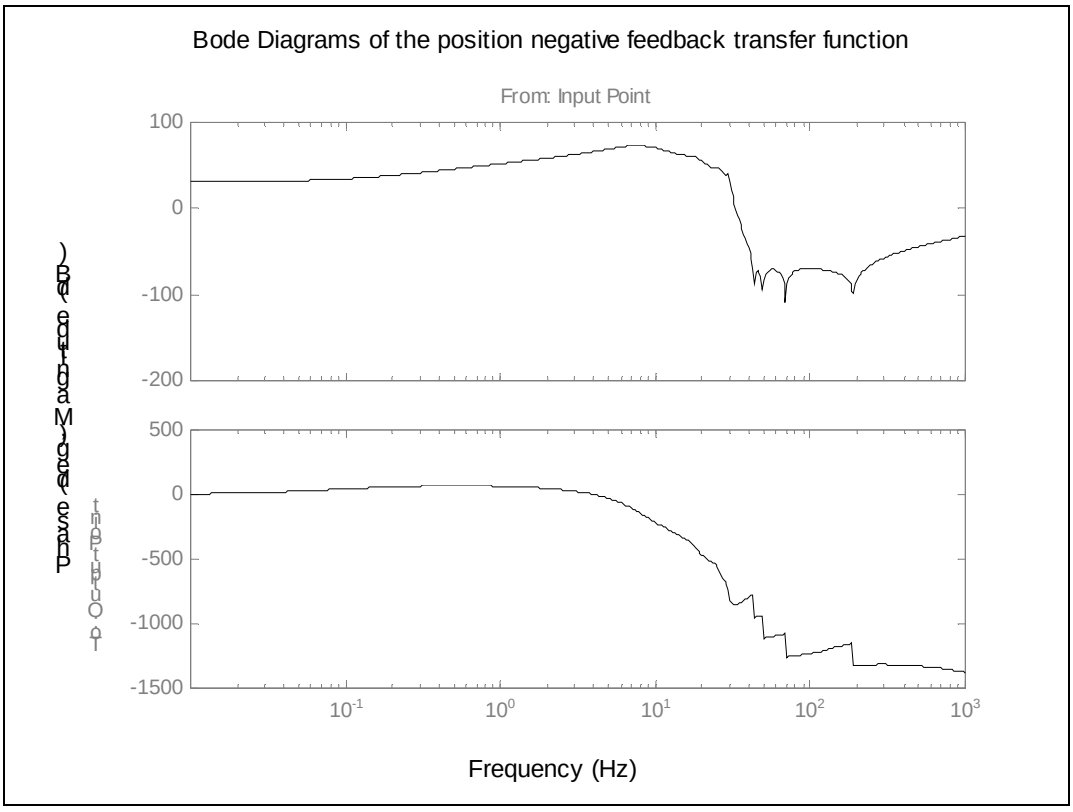

Figure 4.7 Bode diagrams for position negative feedback transfer function

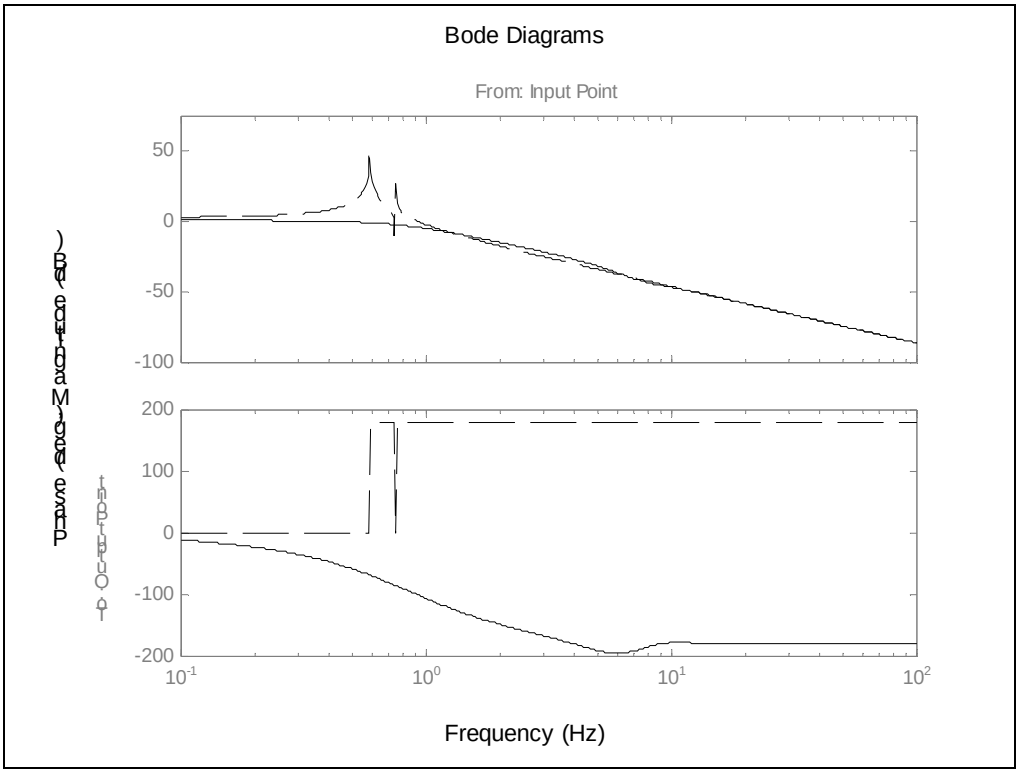

Figure 4.8 Bode diagrams for pitch degree of freedom with (solid) and without (dash) controllers

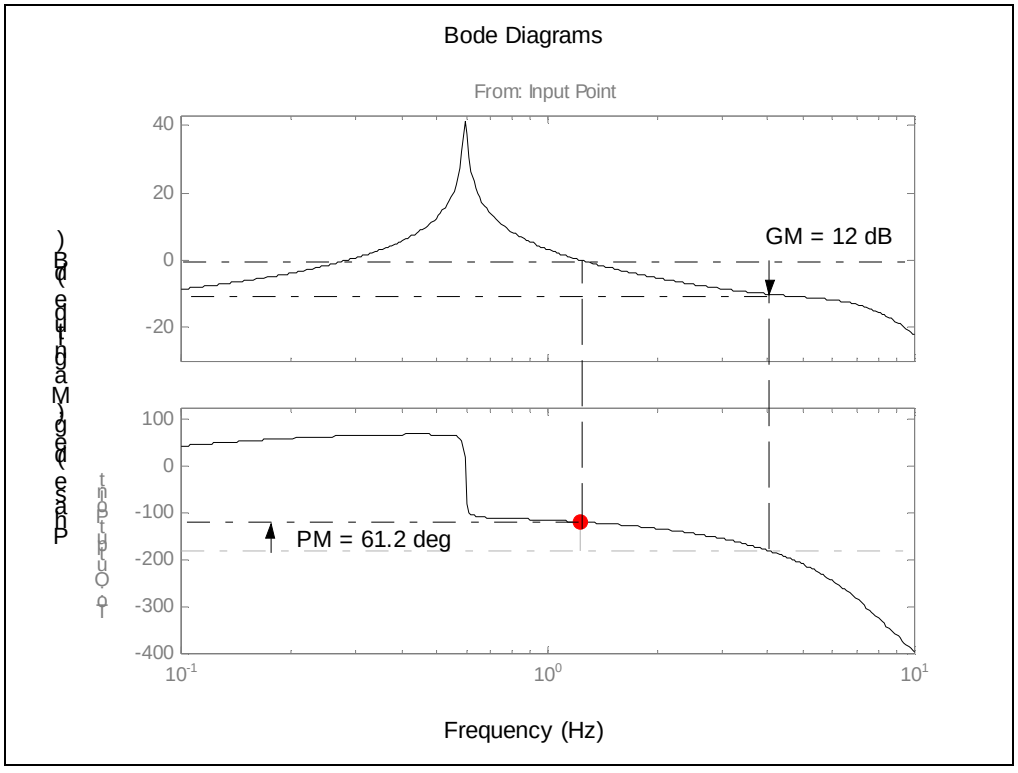

Figure 4.9 Bode diagrams of the pitch open loop transfer function showing stability

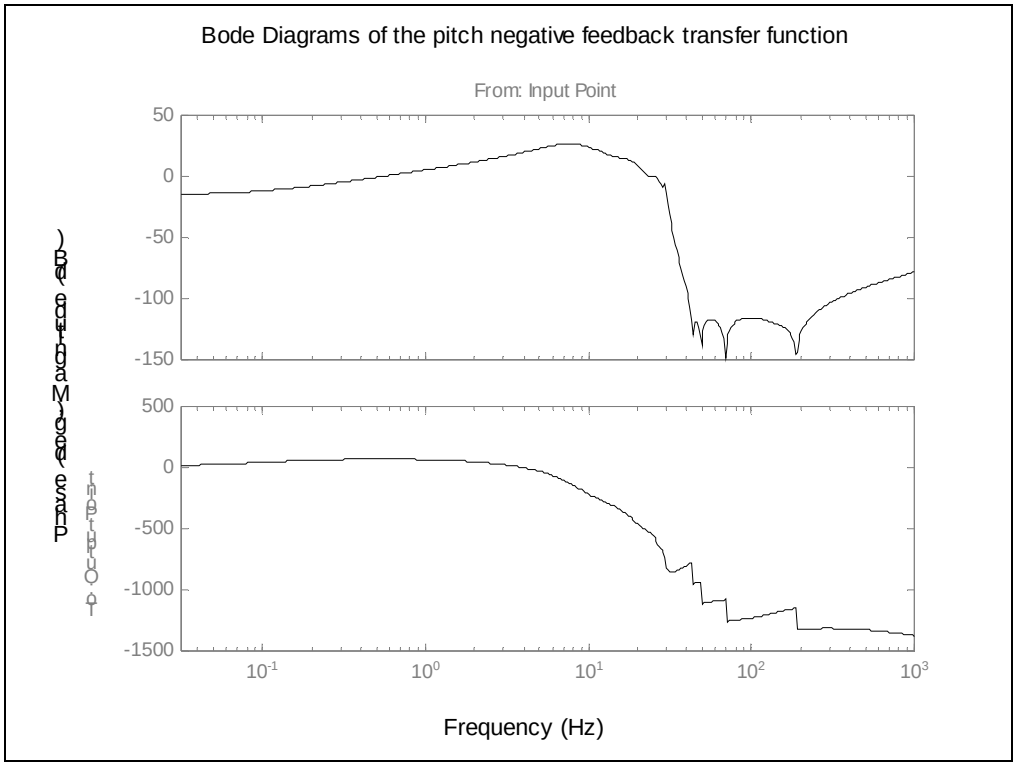

Figure 4. 10 Bode diagrams od the pitch negative feedback transfer function

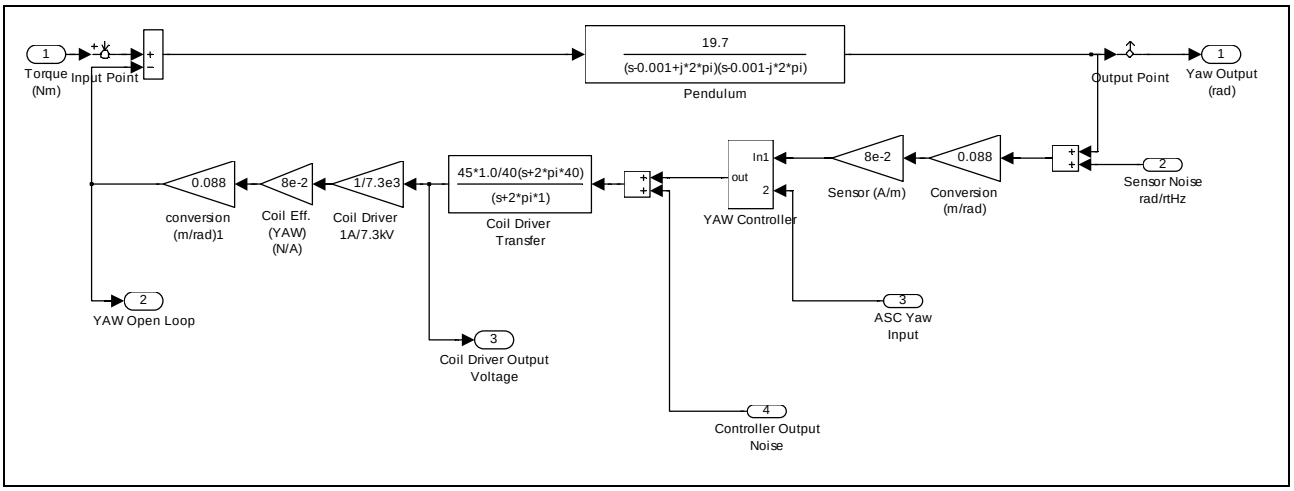

Figure 4.11 LOS Yaw model

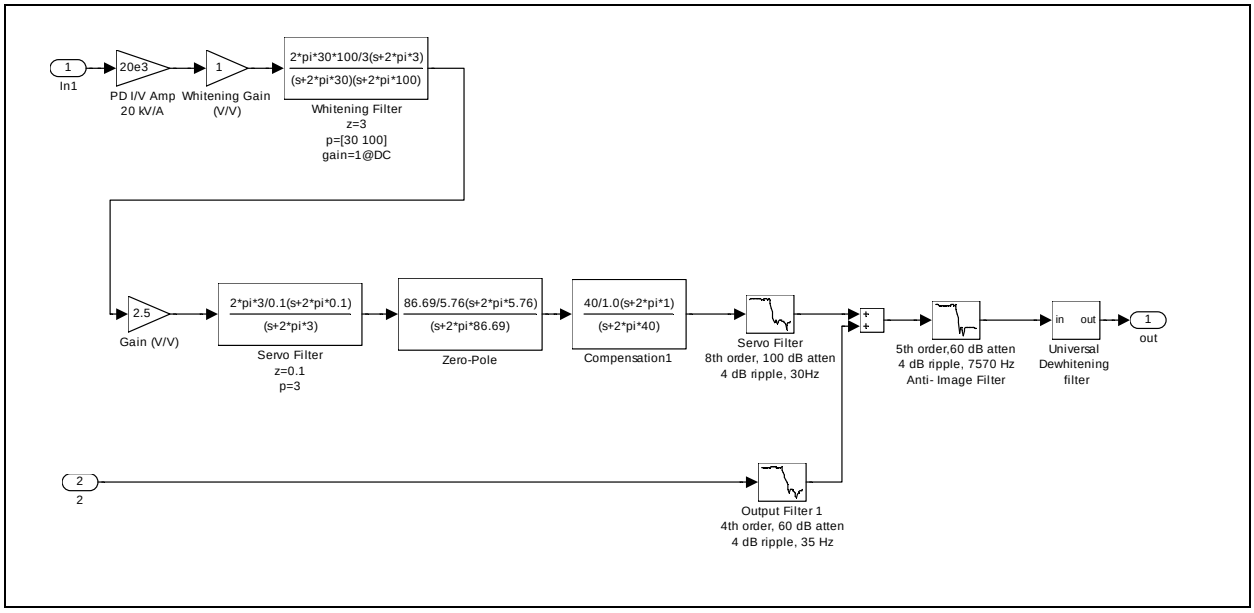

Figure 4.12 LOS Yaw controller

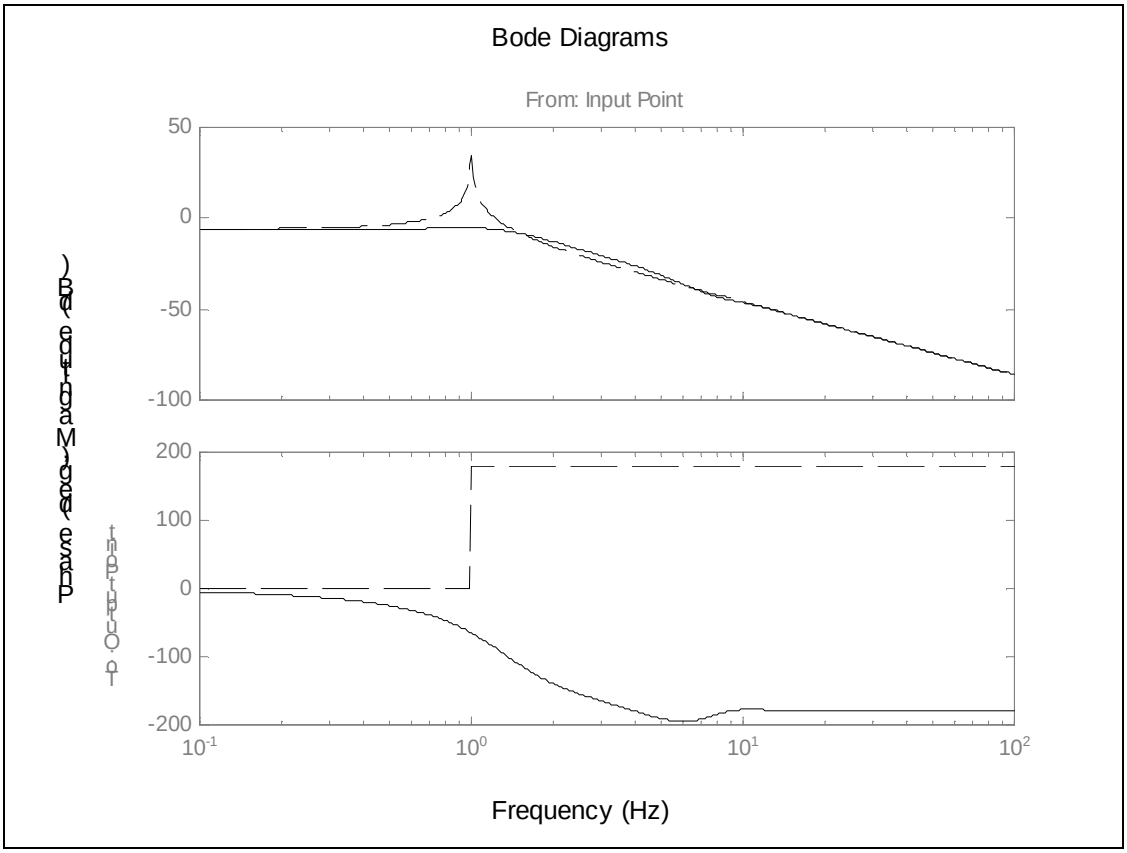

Figure 4.13 Bode diagrams for yaw degree of freedom with (solid) and without (dash) controllers

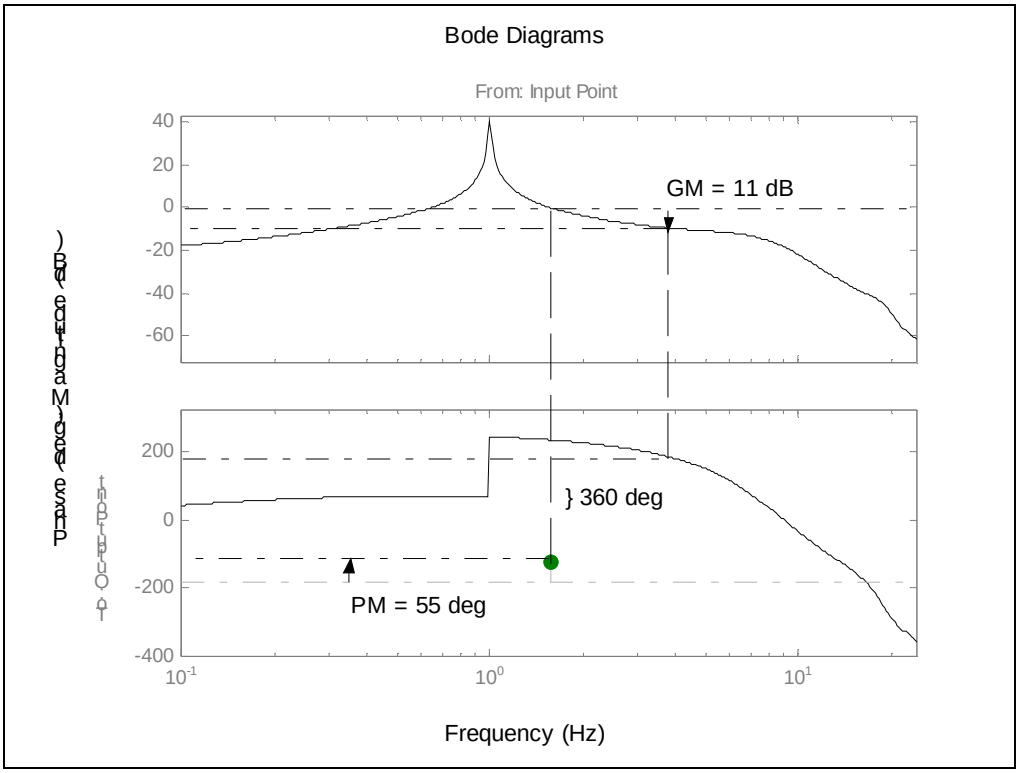

Figure 4.14 Bode diagrams of the yaw open loop transfer function showing stability

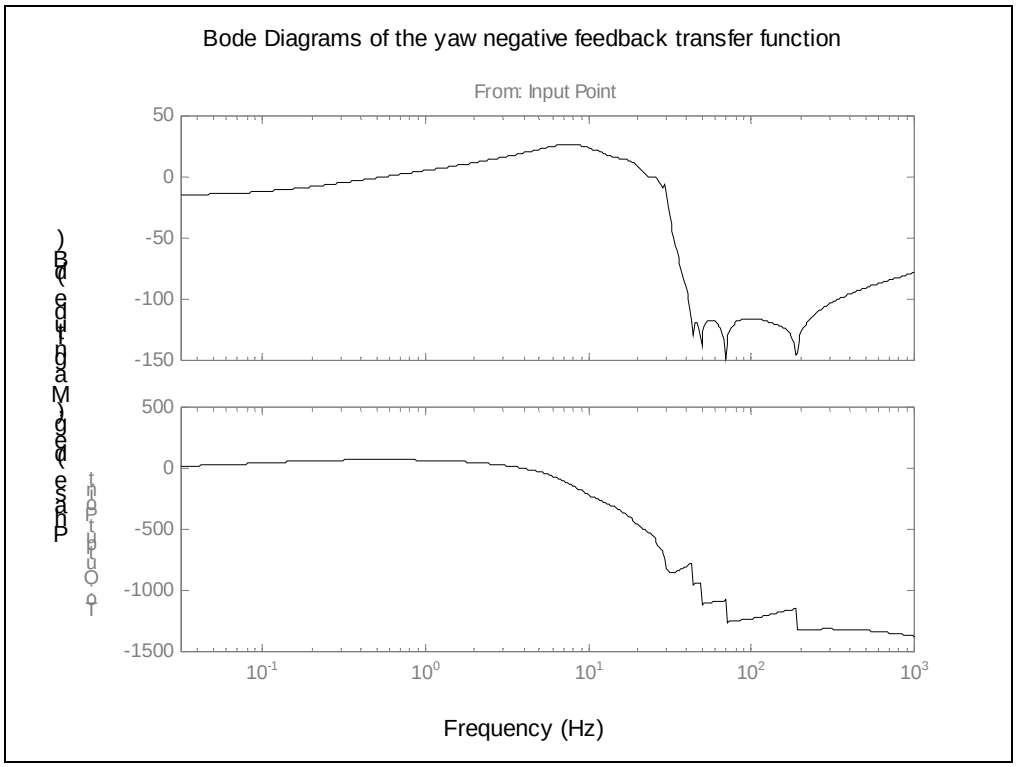

Figure 4.15 Bode diagrams of yaw negative feedback transfer function

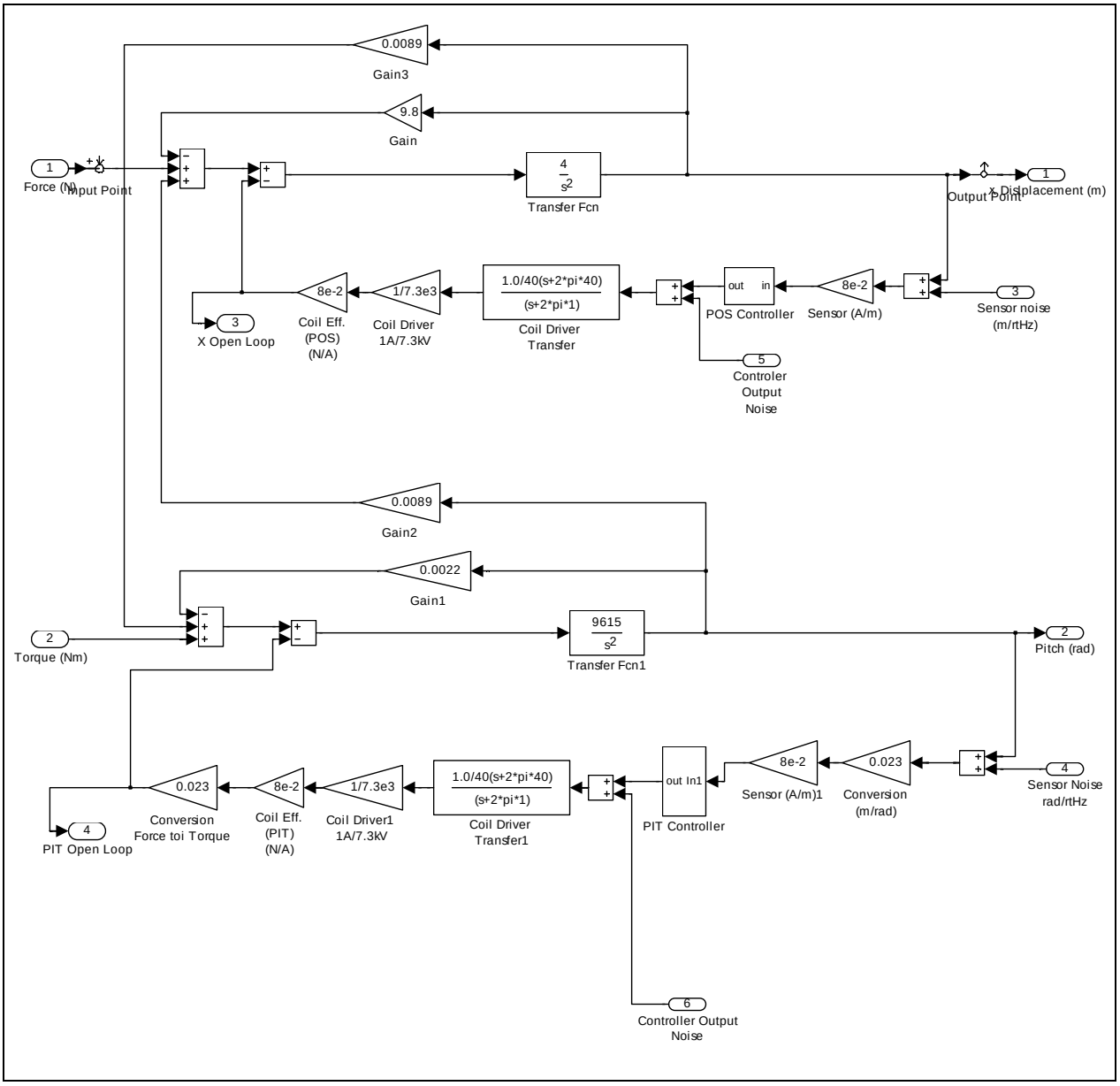

Figure 4.16 SOS Position and Pitch Servo Model

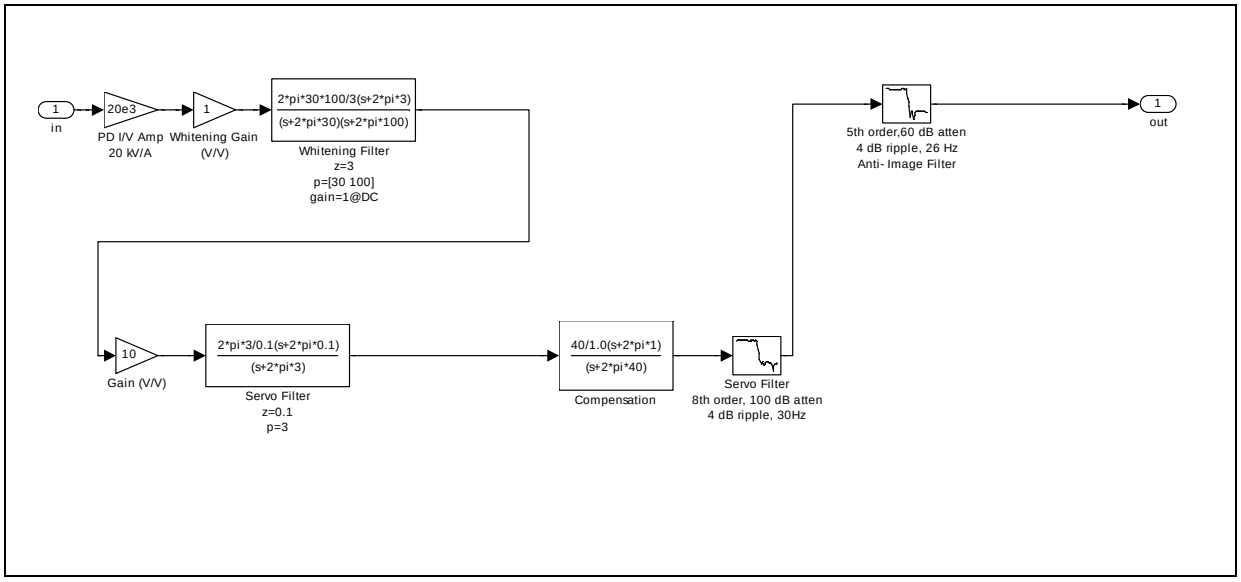

Figure 4.17 SOS Position controller

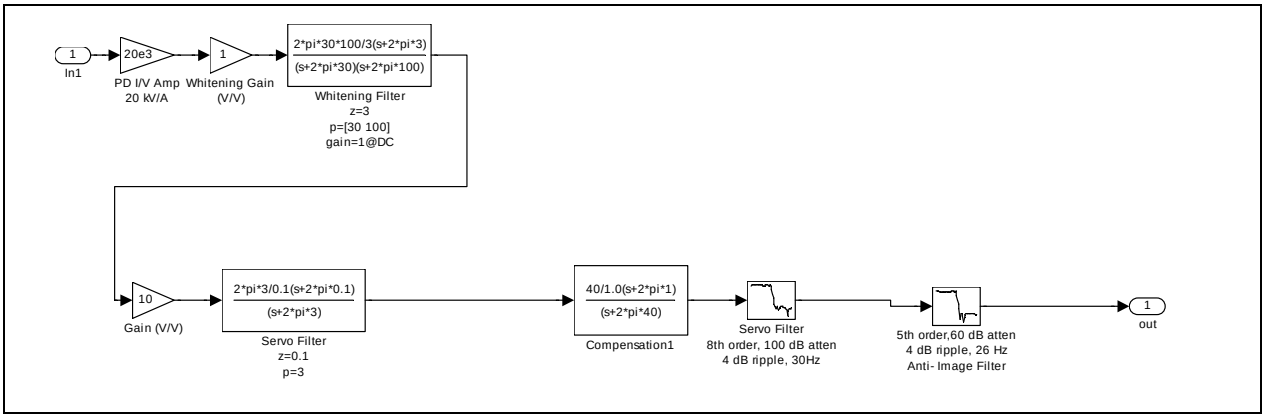

Figure 4.18 SOS Pitch controller

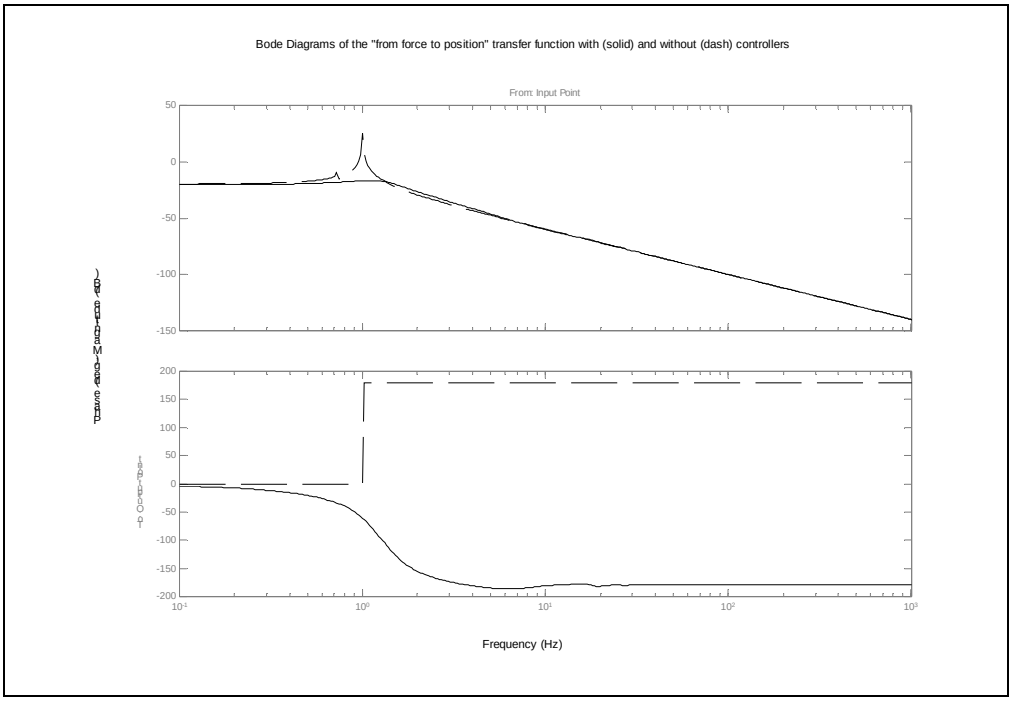

Figure 4.19 Bode diagrams for position degree of freedom with (solid) and without (dash) controllers

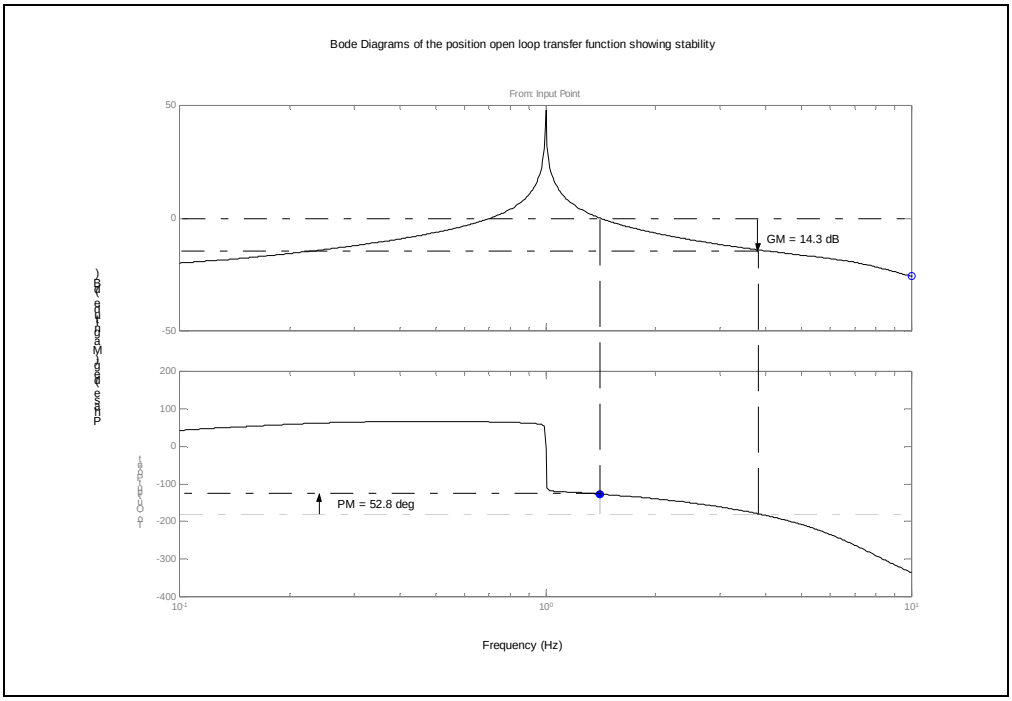

Figure 4.20 Bode diagrams of the position open loop transfer function showing stability

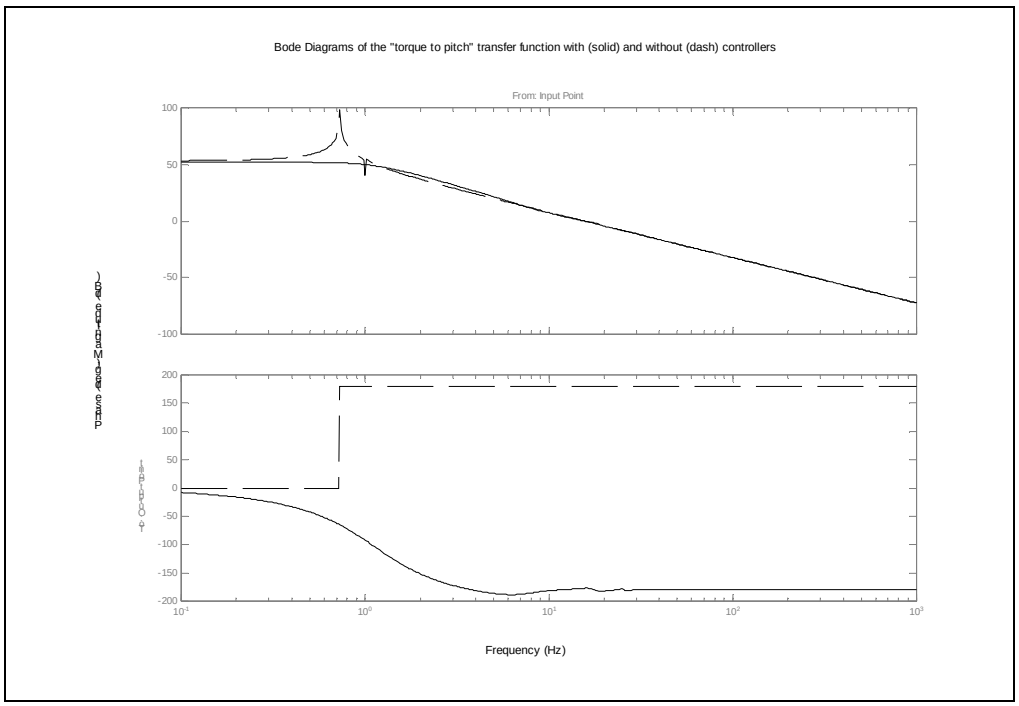

Figure 4.21 Bode diagrams for pitch degree of freedom with (solid) and without (dash) controllers

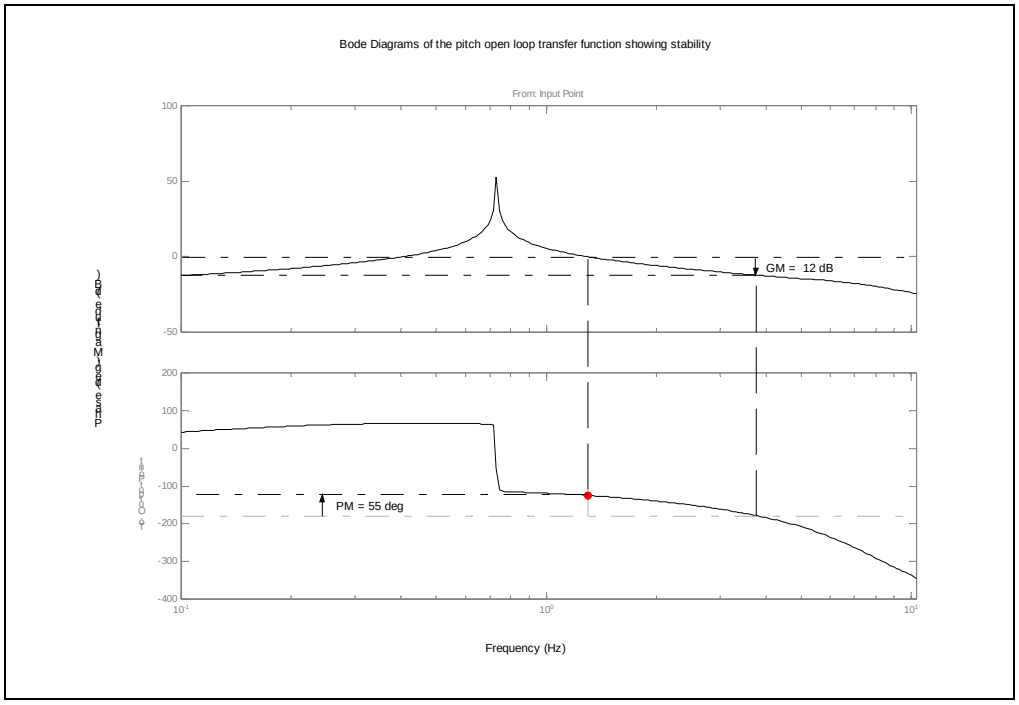

Figure 4.22 Bode diagrams of the pitch degree of freedom showing stability

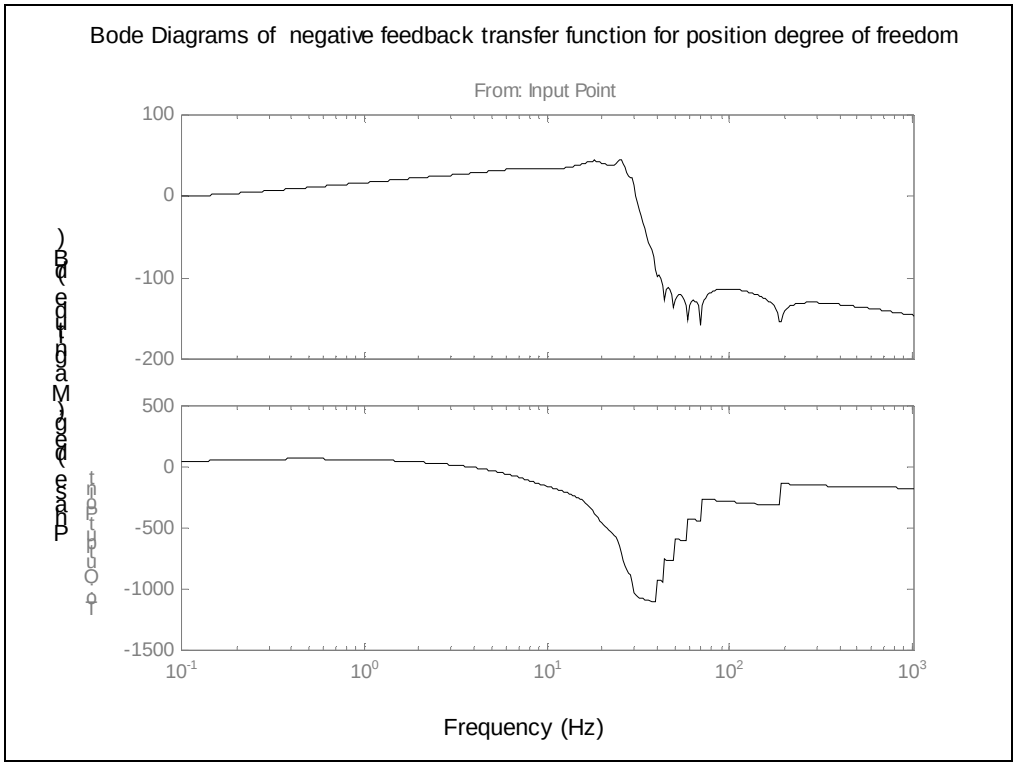

Figure 4.23 Bode diagrams of position negative feedback transfer function

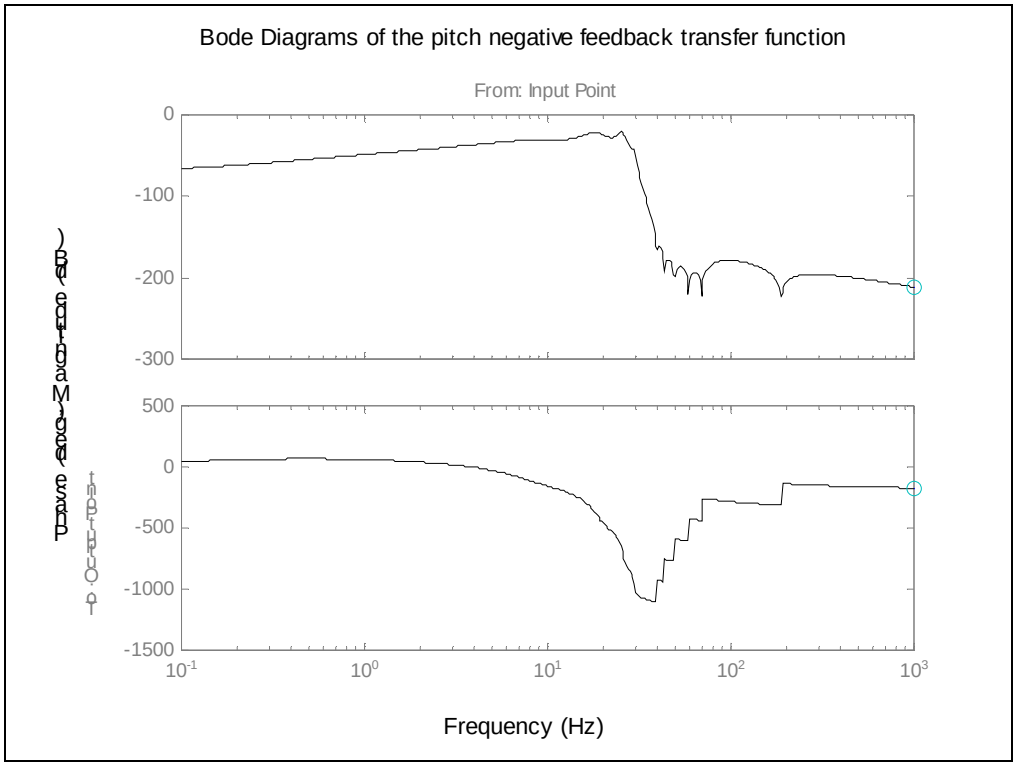

Figure 4.24 Bode diagrams of pitch negative feedback transfer function

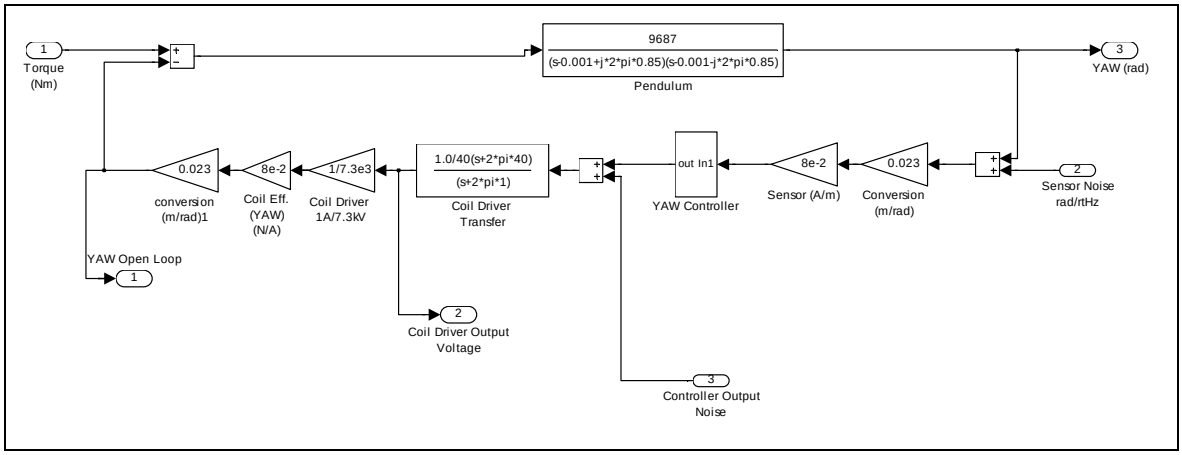

Figure 4.25 SOS Yaw model

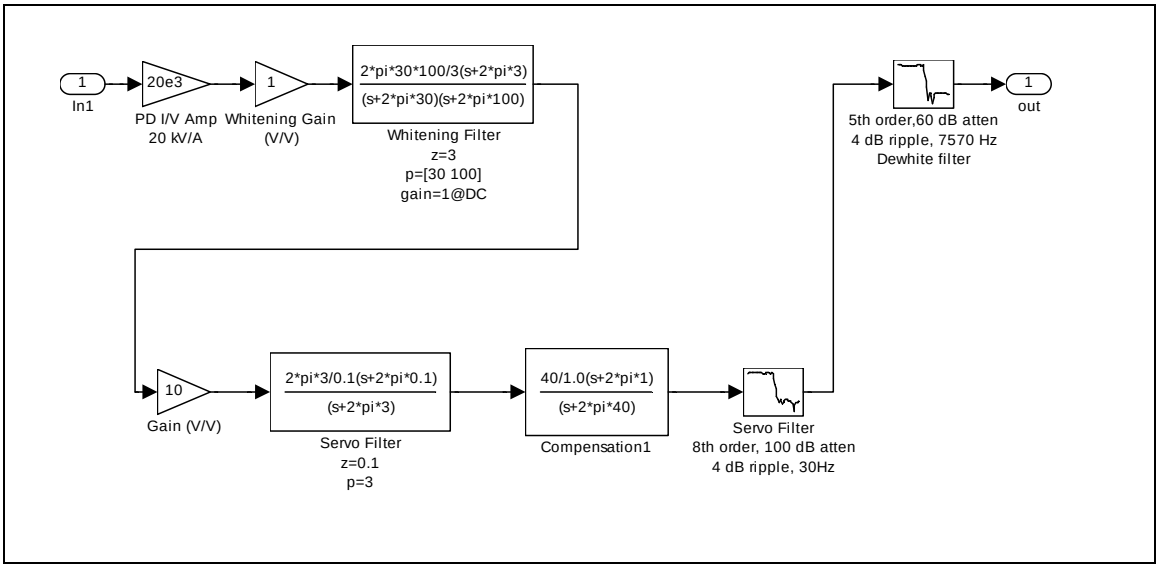

Figure 4.26 SOS Yaw controller

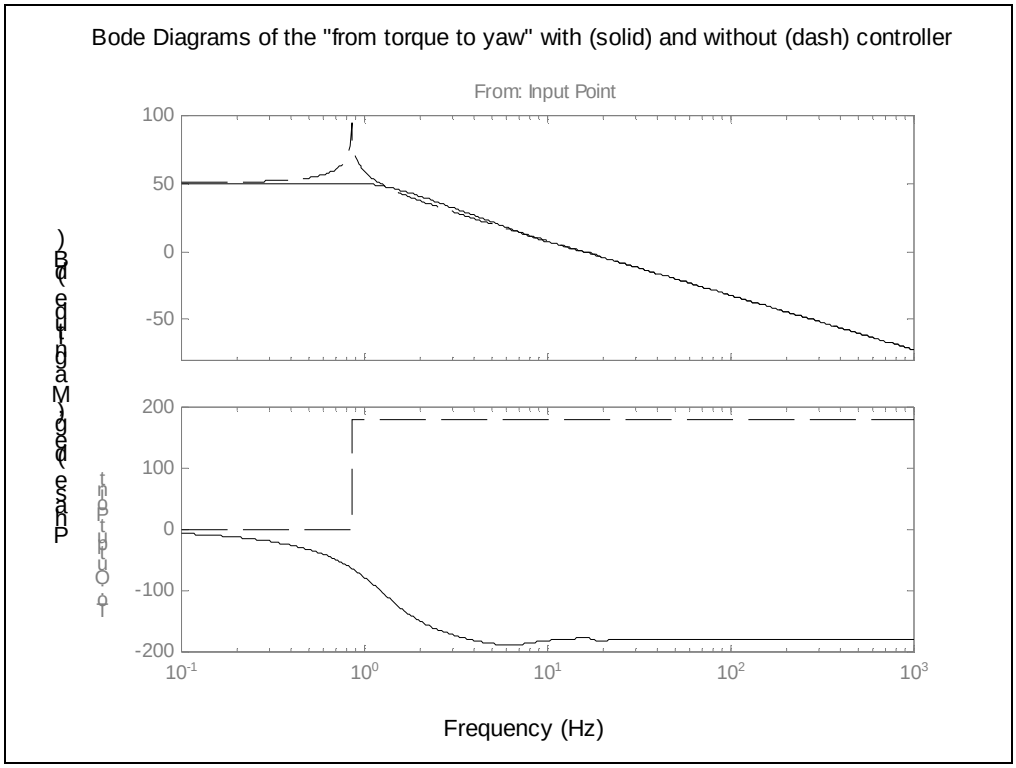

Figure 4.27 Bode diagrams for yaw degree of freedom with (solid) and without (dash) controllers

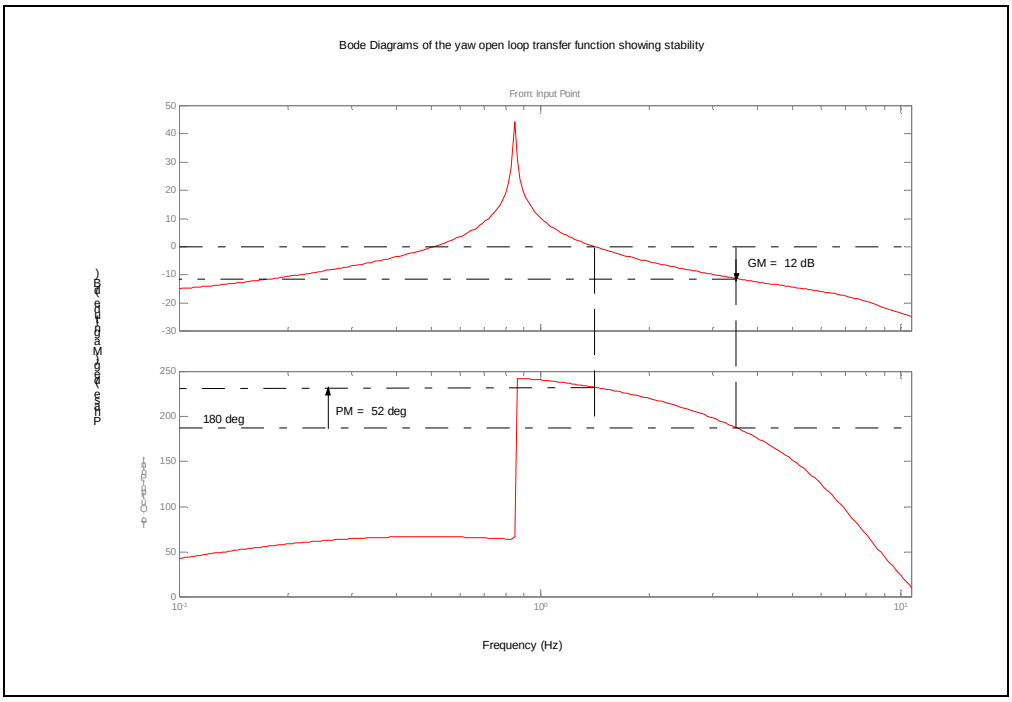

Figure 4.28 Bode diagrams of yaw open loop transfer function showing stability

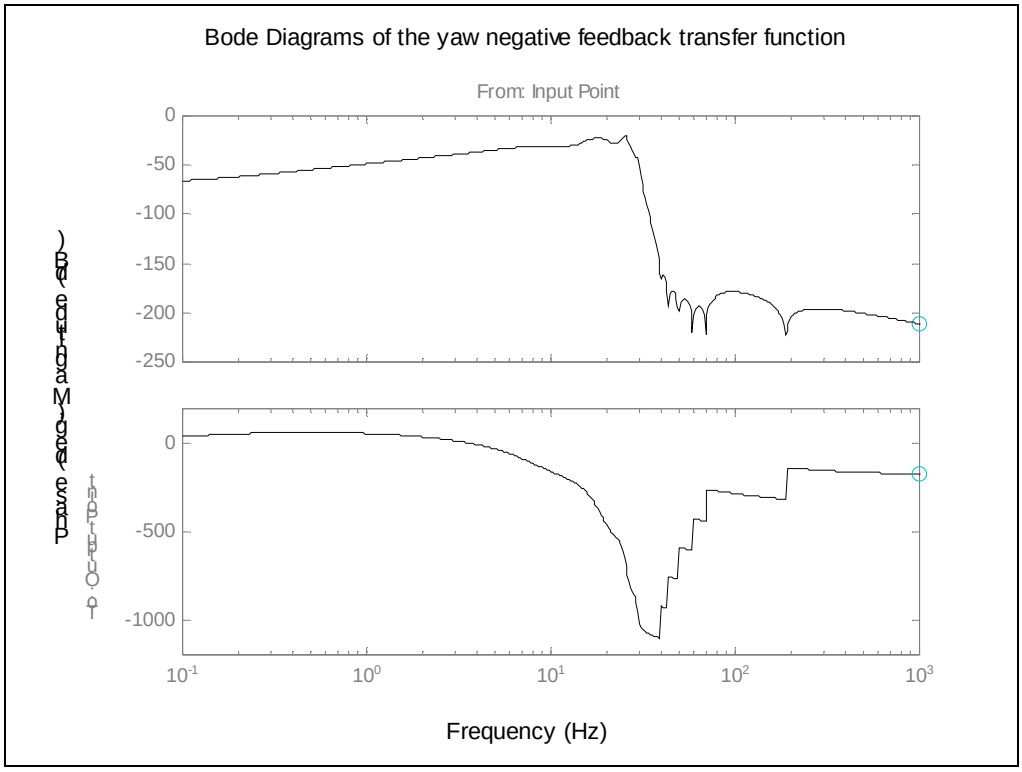

Figure 4.29 Bode diagrams of yaw negative feedback transfer function

5. ELECTROSTATIC DRIVE

Using seismically isolated multiple pendula with coil driver control of higher stages and electrostatic control of the last stage would yield very still test masses. The real point here is that the magnet attachments to the test masses cause thermal noise to dissipate into the LIGO frequency band, so we want to remove these attachments and instead use some actuator that doesn't dissipate thermal energy. Electrostatic drive is a candidate for such actuation. But it has a very small dynamic range, so it is only feasible to employ it on a test mass for which environmental noise is minimized via upper pendulum stages. In this section we will try to address the issue of the electrostatic force acting on suspended test mass -- its intensity for the case of the 40m suspended optics.

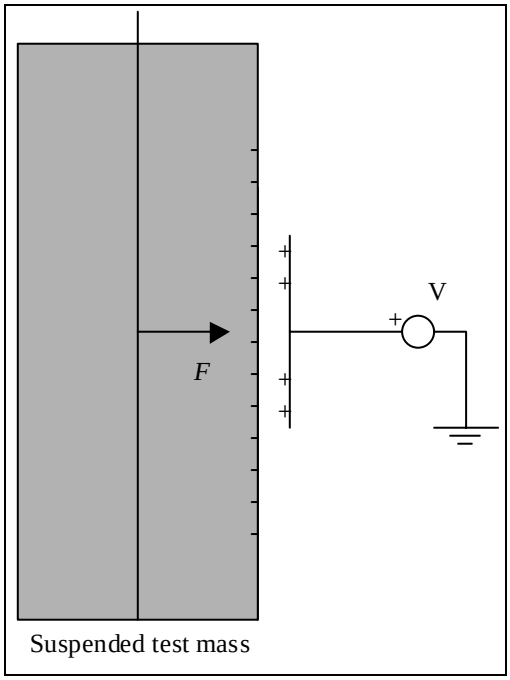

Figure 5.1 Capacitive control of the motion of suspended test mass

When a metal disc, placed very near suspended test mass made of dielectric (fused silica), is charged, this will produce polarized charge on the dielectric surface of opposite sign so there will be electrostatic force acting on a suspended test mass (Fig. 5.1).

If the surface charge density on a metal plate σ is assumed to be homogenous, and the plate is very near to dielectric, not taking into account the edge effect, the electric field between metal plate and dielectric is given by

$$E_1 = \frac{\sigma}{\varepsilon_0}. \tag{5-1}$$

Due to boundary condition, the electric field in the point very near to surface in dielectric will be

$$E_2 = \frac{1}{\varepsilon_r} E_1 = \frac{\sigma}{\varepsilon_0 \varepsilon_r}. \tag{5-2}$$

The induced electric charge σ_r on the dielectric surface causes polarization vector

$$P_2 = -\sigma_r, \tag{5-3}$$

where the sign minus is due to opposite orientation compared to the electric field vector.

From the equation

$$D_2 = \varepsilon_0 E_2 + P_2 = \varepsilon_0 \varepsilon_r E_2, \tag{5-4}$$

we obtain

$$\sigma_r = -P_2 = \varepsilon_0 (1-\varepsilon_r) E_2 = \frac{1-\varepsilon_r}{\varepsilon_r}\sigma. \tag{5-5}$$

If we don't take into account boundary effects, we obtain that the plate is acting on the dielectric with force given by

$$F = \int_{S_2} \sigma_r dS_2 E_2 = \pi a^2 \frac{1-\varepsilon_r}{\varepsilon_r}\frac{\sigma^2}{\varepsilon_0}, \tag{5-6}$$

where *a* is the radius of the metal plate. The charge on the both sides of the metal plate is given by

$$Q = \sigma \cdot 2\pi a^2, \tag{5-7}$$

so the force is

$$F = \frac{Q^2}{4\pi\varepsilon_0 a^2}\frac{1-\varepsilon_r}{\varepsilon_r}. \tag{5-8}$$

The capacitance of the lonely metal disc is given by

$$C = 2\pi\varepsilon_0 a, \tag{5-9}$$

so if we apply the voltage *V* on the metal disc, we will have the attractive force acting on a dielectric with intensity

$$F = \frac{C^2 V^2}{4\pi\varepsilon_0 a^2}\frac{1-\varepsilon_r}{\varepsilon_r} \tag{5-10}$$

Capacitance of the metal disc with radius a = 1" = 2.5 cm is C = 1.4 pF.

The relative dielectric constant of the fused silica is $\varepsilon_r = (1.4)^2 = 1.96$. If we apply voltage of 10 V to the metal disc, the intensity of force acting on the test mass will be

$$F = 1.4 \text{ nN}$$

REFERENCES

[1] Peter R. Saulson, *Fundamentals of Interferometric Gravitational Wave Detectors*, World Scientific, Singapore 1994.

[2] *The Physics of Ligo*, Lecture Notes and Exercises, Caltech 1994

[3] Seiji Kawamura, Jeneen Hazel, Jay Heefner, *Specifications of the 40m Test Mass Suspension Prototype*, an internal working note of the LIGO Project, LIGO-T960162-02-D

[4] J. Heefner, *Large and Small Optics Suspension Electronics Final Design*, an internal working note of the LIGO Project, LIGO-T980043-00-C

[5] Seiji Kawamura, *Response of Pendulum to Motion of Suspension Point*, an internal working note of the LIGO Project, LIGO-T960040-00-D

[6] J. Heefner, R. Bork, *A Digital SOS Control System for LIGO*, an internal working note of the LIGO Project, LIGO-T000068-00-C

[7] J. Heefner, R. Bork, *A Digital LOS Control System for LIGO*, an internal working note of the LIGO Project, LIGO-T000010-A1-C

[8] J. Heefner, R. Bork, *A Digital LOS and SOS Control Systems for LIGO*, an internal working note of the LIGO Project, LIGO-T000073-00-C

[9] P. Fritschel, J. Heefner, *DAC Output Signal Conditioning: Dewhitening and Anti-imaging filter design*, an internal working note of the LIGO Project, LIGO-T000074-00-D

CONTENTS

1. Introduction 1

1.1 The equations of motion for position and pitch degrees of freedom of a suspended mirror 2

1.2 The equations of motion for yaw degree of freedom of a suspended mirror 4

1.3 The 40m test mass and suspension configuration 6

1.4 Simulink model of a pendulum 8

2. Control system design 16

2.1 General description of the 40m suspension control system 16

2.2 Block diagram of control system 20

3. Simulink modeling of the 40m pendulum control system 24

3.1 Position and pitch degrees of freedom 24

3.2 Yaw degree of freedom 28

3.3 Time response 31

4. Simulink modeling of a digital LOS and SOS control system for LIGO 34

5. Electrostatic drive 50

References 52

Contents 53